WELDING
INSTITUTE OF
CANADA

INSTITUT
DE SOUDAGE
DU CANADA

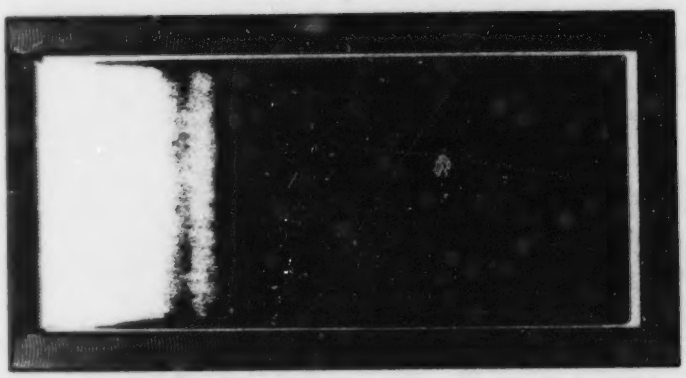

HEAD OFFICE:

391 BURNHAMTHORPE ROAD EAST/OAKVILLE, ONTARIO L6J 6C9

TELEPHONE: (416) 845-9881

WELDING INSTITUTE OF CANADA
INSTITUT DE SOUDAGE DU CANADA

391 BURNHAMTHORPE RD EAST OAKVILLE, ONTARIO L6J 6C9 TELEPHONE (416) 845-9881

October 20, 1980

FINAL REPORT

BY

Robert B. Lazor

STUDY OF WELD CRACKING IN HIGH STRENGTH LOW ALLOY STEELS

APR 5 1984

MICROMEDIA

Report No. RC13/80

Approved by:

Dr. N.F. Eaton
Director General

85pp

DSS File Number: 14SQ.23440-8-9073

DSS Contract Serial No: ISQ78-00186

Canmet Project No:8-9073

Canmet Scientific Authority:
Dr. J.T. McGrath

ABSTRACT

A study was conducted to investigate hydrogen-induced delayed failure of high-strength, low alloy steels. Weld metal cracking was examined using the gapped-bead-on-plate (G-BOP) test and heat-affected zone cracking was studied with a modifed version of the implant test. The crack susceptibility of actual weld joints was determined from a small-scale, high-restraint test, and information on reaction forces was obtained from another series of instrumented restraint tests.

The results of the weld metal cracking tests showed that niobium diluted from the baseplate significantly raised the preheat required to avoid weld metal cracking. Preliminary tests using the modified implant technique have shown that C, Mn, and Mo are detrimental to HAZ cracking; these results support previous work on cracking in the heat-affected zone.

The high-restraint tests on butt welds confirmed the increase in crack susceptibility due to the presence of niobium in the base plate and it was noted that the dilution of niobium into the weld promoted root bead cracking. Results of the instrumented restraint tests showed that considerable bending occurs in most cases which drastically lowers the effective reaction forces. The reaction forces were not considered to be influenced by the preheating temperature so that the only effect of preheating is to reduce the resultant weld metal hydrogen content and thus lower the crack susceptibility.

ACKNOWLEDGEMENTS

The Welding Institute of Canada would like to thank the Department of Supply and Services, Canada for their financial support and Dr. J.T. McGrath of Energy, Mines and Resources, Canada who acted as scientific authority for this project.

The author wishes to thank Mr. G. Campbell and Mr. N. Sweetman for their help during the experimental portion of this program and Mr. W. Fearis and his staff who prepared the machined specimens.

The technical supervision and editorial comments of Mr. B. Graville are greatly appreciated.

TABLE OF CONTENTS

		Page
	Abstract	ii
	Acknowledgements	iii
	List of Tables	v
	List of Illustrations	vi
1	Introduction	1
2	Experimental	3
	2.1 Materials and Welding Procedures	4
	2.2 Weld Metal Cracking Tests	5
	2.3 Heat Affected Zone Cracking Tests	5
	2.4 Y-groove High Restraint Cracking Tests	8
	2.5 Instrumented Restraint Cracking Tests	9
3	Results and Discussion	10
	3.1 Weld Metal Composition	10
	3.2 Weld Metal Cracking Tests	11
	3.2.1 Hydrogen Diffusion Model	12
	3.2.2 Effects of Composition	14
	3.3 Heat Affected Zone Cracking Tests	17
	3.4 Y-Groove High Restraint Cracking Tests	19
	3.4.1 Intensity of Restraint	20
	3.4.2 Chemical Composition	21
	3.5 Instrumented Restraint Cracking Tests	23
	3.5.1 Measurement of Reaction Forces	24
4	Conclusions	28
	References	30
	Appendix A - Modified Implant Calibration	55
	Appendix B - G-BOP Results	59
	Appendix C - Statistical Analysis of Weld Metal Cracking Tests	70
	Appendix D - High Restraint Cracking Results	74

LIST OF TABLES

		Page
Table 1	Composition of Steels and Consumables	32
Table 2	Summary of Results of Weld Metal Cracking Tests	33
Table 3	Calculation of Integrated Diffusion Coefficient for Various Temperatures	34
Table 4	Strengthened Implant Cracking Percentages	35
Table 5	Summary of Results of Restraint Tests	36

A STUDY OF WELD CRACKING IN HSLA STEELS

1. INTRODUCTION

The incidence of hydrogen cracking in the heat-affected zone of modern high-strength low-alloy (HSLA) steels has been reduced compared to the incidence in earlier steels by decreasing the carbon content. The mechanical properties of HSLA steels are obtained by grain refinement and precipitation hardening instead of pearlite content as in the earlier steels[1]. However, cracking is still encountered under some circumstances, particularly when high hydrogen processes are used or where the weld is highly restrained. The improved resistance of the steels to heat-affected zone cracking implies that the crack resistance of the weld metal must also be considered. In the past, the carbon level in the weld metal was usually much lower than the base material. If cracking occurred it usually took place in the HAZ, but since other strengthening mechanisms are available for HSLA steels, the weld metal often has the higher alloy content and is more prone to cracking. Furthermore, because of dilution effects, the composition and subsequent susceptibility to cracking of root runs of butt welds are strongly influenced by the alloying elements of the parent material. The weld metal cracking susceptibility resulting from a given electrode may, therefore, be influenced by the steel being welded.

Hydrogen cracking, or cold cracking, is avoided by selecting a suitable preheat or postheat cycle for the particular steel being welded. On large

LIST OF ILLUSTRATIONS

		Page
Figure 1	The gapped bead-on-plate (G-BOP) Test	37
Figure 2	The Modified Implant Test	37
Figure 3	Strain gauged Modified Implant Specimen	38
Figure 4	Small Scale High Restraint Cracking Test Assembly	39
Figure 5	Method of Measuring Percentage Cracking in Restraint Tests	40
Figure 6	Instrumented Restraint Test Assembly Showing Completed Root Weld.	41
Figure 7	Weld Metal Cracking Percentage vs. Preheat Temperature from G-BOP tests	42
Figure 8	Weld Metal Hydrogen Content vs. exposure Time at 90% Relative Humidity for Basic Electrodes	43
Figure 9	Plot of τ against Preheat Temperature	44
Figure 10	Relationship between $\log_{10}(H_f)$ and τ_c for Steel 133	45
Figure 11	Relationship between $\beta\tau_c - \log_{10}(H_f)$ and Chemical Composition	45
Figure 12	Manganese Content vs. Critical Preheat temperature	46
Figure 13	Cracking percentage vs. Preheat Temperature for High Restraint Tests	47
Figure 14	Cross-Sections of Cracked Restraint Test Welds	48
Figure 15	Relationship between reaction force and time after start of welding	
	(a) welds made at room temperature, high restraint	50
	(b) preheat of 60°C above room temperature, high restraint	51
	(c) preheat of 100°C above room temperature, high restraint	52
	(d) welds made at room temperature, low restraint	53
Figure 16	Comparison of calculated and measured reaction forces for instrumented restraint tests	54

construction jobs this usually involves the fabrication of special facilities, which can be very expensive. Small differences in the crack resistance of the parent metal or weld metal may be useful to reduce costs significantly. It is, therefore, imperative that there be available means of assessing and predicting crack resistance.

The crack susceptibility of the HAZ has previously been measured using simple carbon equivalent formulae, a list of which may be found in an article by Ito and Bessyo[2]. In high carbon steels, the CE gives a reasonable measure of hardenability and indicates the probability of forming a hard HAZ susceptible to cracking. The CE is misleading for HSLA steels because many elements have a pronounced effect on hardenability, but may not influence the cracking susceptibility. The inadequacy of a CE for HSLA steels may result from a gradual change in the nature of the martensite from internally-twinned individual martensite plates at high C contents to low carbon 'lath' or 'slipped' martensite, containing high dislocation densities[3]. The question also exists as to whether the effects of certain elements on HAZ cracking will be similar on weld metal cracking. A susceptibility parameter which applies to both the WM and HAZ for HSLA steels would be desirable. Before such a parameter can be developed there is the need to develop a more thorough understanding of weld metal and HAZ cracking, and their interaction in low carbon materials, particularly under conditions of high hydrogen and high restraint.

The objectives of this program were to study the effect of;

1. steel composition on HAZ cracking susceptibility,
2. weld metal composition on weld metal cracking, and
3. investigate the cracking behaviour in actual welds joints for modern low carbon HSLA compositions

The results will be useful in producing a scheme for predicting weldability and the selection of consumables and welding procedures.

2. EXPERIMENTAL

The G-BOP (gapped bead-on-plate) test and modified implant test were used for weld-metal cracking and heat-affected-zone cracking studies, respectively.

The design of the G-BOP test is shown in Figure 1. In this procedure, two blocks of steel, one with a recess machined in it, were clamped together to provide a slit over which the test bead was laid. After allowing 24 hours for cracking to occur, the weld over the gap was heated causing any crack surfaces present to oxidize. When the blocks had cooled, they were broken apart, and any cracking appeared as a blue thumbnail. Complete details of this test may be found in the literature[4,5].

The modified implant test is shown in Figure 2. The implant was loaded to a constant value by tightening the nut to a given torque, torsion being eliminated by a thrust bearing. After allowing time for cracking, the weld

was heated to oxidize any crack surfaces present. As with the G-BOP test, a series of tests at various preheat levels will establish the critical preheat to avoid cracking.

The crack susceptibility of actual weld joints was measured using two types of tests. One was a Y-groove restraint test, which had a fixed level of restraint, and the other was a larger restraint test in which the reaction stress was measured and the restraint quantified.

2.1 Materials and Welding Procedures

Ten experimental steels, compositions of which are shown in Table 1 were cast and forged into billets, from which G-BOP blocks were machined. The exact size of the blocks varied slightly because the ingot sizes were nonuniform; the approximate dimensions were 90 x 90 x 50mm high.

Welds were deposited automatically using 4mm diameter E6010 and E7018 electrodes. The welding conditions for the E6010 and E7018 electrodes were 128A, 25V, 25.4 cm/min. and 128A, 25V, 25.4 cm/min, respectively. The resultant heat inputs were 7.6 kJ/cm and 8.5 kJ/cm, respectively.

The low-hydrogen (E7018) electrodes were exposed at 90% relative humidity for various lengths of time to vary the resultant weld metal hydrogen content. Sufficient electrodes were placed in the humidity cabinet so that the hydrogen in the weld metal was determined for similar exposure conditions as the electrodes used for the G-BOP tests. The hydrogen

was measured using mercury as the confining fluid as outlined in ISO Standard ISO 3690-1977 (E)[6].

2.2 Weld Metal Cracking Tests

The welds were deposited onto the G-BOP blocks, which were preheated at various temperatures up to 200°C. The blocks were superheated about 30°C above the desired preheat and allowed to cool slowly until the exact temperature was reached. They were then welded and allowed to cool to room temperature in still air. After allowing 24 hours for any cracking to occur, the weld area was heat tinted and later broken apart to determine if any cracking had occurred.

The cooling behaviour of the G-BOP blocks was measured using a digital thermometer and a recorder. The thermocouple for the digital thermometer was inserted into a hole predrilled into one of the blocks. A Pt-Pt/13% Rh thermocouple (type R) connected to the recorder was inserted into the molten weld pool and allowed to solidify 'in situ' to monitor the preliminary cooling of the weld. The initial weld thermal cycle was obtained from the recorder output while the cooling behaviour below the preheat temperature was monitored using the digital thermometer.

2.3 Heat-Affected Zone Cracking Tests

When G-BOP tests had been completed, the blocks were used to machine implant specimens of the dimensions given in Figure 2. The longitudinal

axis of the implants was parallel to the rolling direction.

A modified implant test using one level of stress with various preheats was developed during this investigation. The principle behind the test is similar to a G-BOP test in that heat tinting is used to measure the amount of cracking as a function of preheat temperature.

The load was applied to the implant 5 minutes after welding by tightening the nut (see Figure 2) to a specified torque. A thrust bearing was used to eliminate any residual torque and the threads were lubricated to reduce friction between threads. The strain produced in the implant specimens as a function of torque was measured using a strain-gauged sample (see Figure 3). It was found that the relationship between stress and torque was given by:-

$$\sigma = .0308\ T \qquad \text{where } \sigma = \text{stress, kg/mm}^2$$

$$T = \text{torque, mm-kg}$$

Details of the calculations are found in Appendix A.

Various combinations of nuts and thrust bearings were tested on the strain-gauged sample at one level of torque to ensure that variations in stress caused by different nuts was within $\pm$10% of the expected value. The range of stresses obtained was considered adequate for this application.

The main problems encountered during the development of the modified implant test were to produce cracking in the HAZ and to ensure that results were comparable amongst the alloys. The low alloy content of the materials results in low hardenability as calculated from a conventional carbon equivalent formula. The heat-affected-zone in similar steels is relatively soft and has a low susceptibility to delayed cracking. Even without preheat and using cellulosic electrodes it was difficult to achieve consistent cracking results. Most of the preliminary implants yielded in the threads below the HAZ after considerable elongation and thus these results were not particularly useful. However, they did point out that there was a considerable range of yield stresses in these materials. In order to examine the influence of yield stress on HAZ cracking pairs of samples from the first 5 steels were welded. The first implant was torqued until it yielded and the second was torqued to just below yield. Weld code nos. 2, 5, 9, 11 and 14 were torqued to yield and 3, 6, 10, 12 and 15 were loaded just below yield. Except for weld code no. 11, the first set of implants were essentially 100% broken and the ones tested below yield had cracking percentages from 20 to 100%, but not all of them were clearly broken through the HAZ. Therefore all steels were tested at a higher load to promote cracking (31 kg/mm^2) and to give comparable results. However, problems of yielding in the threads below the HAZ were still encountered.

This obstacle was overcome by austenitizing the implants and quenching immediately into water to increase the hardness and crack susceptibility before welding. Although steels are not usually quenched before welding this method was used only to promote cracking so that a comparison can be made of the results.

2.4 Y-Groove High Restraint Cracking Tests

A high-restraint cracking test was conducted using two different edge preparations; one was a sloping Y-groove as used in a Tekken test and the other was a straight Y-groove. The sloping Y-groove promotes HAZ cracking, whereas the latter may crack in either the weld metal or heat affected zone. Both edge preparations were compared on steel 13A and it was decided to continue the remaining tests usdng a straight Y-groove since cracking was allowed to propagate in either WM or the HAZ for this configuration.

The small-scale high-restraint cracking test assembly is shown in Figure 4. The welds along the top edges are of sufficient size to resist the shear stress caused by the weld contraction across the gap while the stiffener along the bottom edge ensures that the ends do not rotate as the weld cools.

The welding conditions were changed from those used for the C-BOP tests because of variations in the arc caused by welding in a groove compared

to the flat plate. The new settings were as follows: 120A, 26V, 25.4 cpm for E6010 (7.37 kJ/cm) and 160A, 24V, 31.3 cpm for E7018 electrodes (7.36 kJ/cm).

Preheating was accomplished by placing the complete restraint assembly in the oven and allowing the assembly to cool slowly in still air before welding. After 24 hours, the centre sections of the test pieces were removed and metallographically examined on six surfaces from each weld. The lengths of the cracks, if cracking occurred, were measured and it was noted whether the cracking was predominantly through the weld metal or heat-affected zone. The degree of cracking is characterized by values which determine the crack sensitivity in a cross-section and the crack sensitivity in the root of a weld. These values are the same as those specified by Kihara et al[7] and are shown in Figure 5.

The cooling behaviour of these restraint tests were measured at a distance of 6.5mm from the weld bead using a Pt-Pt/13% Rh thermocouple. Although the peak weld temperatures were not obtained, the rate of loss of preheat was accurately determined.

2.5 Instrumented Restraint Cracking Tests

The instrumented restraint tests were conducted using the same edge preparation and welding conditions as the self-restrained tests. A view of the test assembly with a completed weld is shown in Figure 6. The strain gauged sidearms serve a dual purpose. Machined faces on the

restraint arms and the test specimen ensured that a 2mm gap was maintained across the weld preparation by tightening the nuts prior to welding. The reaction strains were measured using a strain gauge half bridge on each sidearm. The Poisson gauges provided complete temperature compensation when the samples were preheated; the strain gauges and accompanying materials were able to withstand short term temperatures of 250°C.

The cooling behaviour below 200°C was recorded using chromel/alumel thermocouples located 6mm from the weld in the base material. Thermocouples inserted in the actual weld have been found to promote cracking in some instances[8] and thus were avoided in the present program. The strains were recorded as the weld cooled and later converted to reaction stresses. The crack sensitivity of the weld was determined as shown in Figure 5 from sections on each weld, thus providing information on the effects of preheat on crack susceptibility.

3. RESULTS AND DISCUSSION

3.1 Weld Metal Composition

The chemical compositions of the G-BOP test welds were obtained by analyzing drillings removed from the top of the weld beads. The results of the analyses are included in Table 2. Silicon was not expected to change very much due to welding and was measured only for weld 133. A comparison of the compositions of the base material and

the weld beads showed that the carbon and silicon contents do not change significantly but the other alloying elements have various recoveries: 50% for Mn and V, 65% for Mo and Nb, and 60% for Ni. These recoveries are comparable to dilution of alloying elements from the base material for submerged arc welds[9,10]. The chemical analyses were done on welds deposited with E6010 electrodes. It is expected that welds made using E7018 electrodes would have slightly higher Mn contents, but would be otherwise similar.

3.2 Weld-Metal Cracking Tests

The results of the G-BOP tests, showing the relationship between crack susceptibility and preheat temperature, are presented in Figure 7. Complete test results are shown in Appendix B for each complete composition. Except for steel 133, the slopes of the lines are approximately the same for both the low and high hydrogen conditions. The results for each steel are characterized by the critical preheat to avoid cracking, T_c. This temperature was obtained by noting the point where a line with a slope of-2 drawn through the curves of Appendix B intersected the abscissa. For steels with different curves the characteristic line used to measure T_c was drawn through the cracking vs. preheat plot at 50% cracking.

The hardness of welds deposited without preheat are also included in Table 2. The effect of preheat on hardness was determined for steel 139 by welding at a 200°C preheat; the hardness of this bead was 251 (DPH_{30})

compared to 288 (DPH_{30}) when welded at room temperature. One would expect that preheating the blocks would decrease the cooling rate so that the hardness would be considerably lower. However, hardening curves for steels of similar compositions[8] do not exhibit a great effect on maximum HAZ hardness with changes in cooling rate. Since the heat-affected zone hardness is insensitive to welding conditions it may be argued that likewise, the weld metal hardness is not greatly affected by the preheat temperature.

The hydrogen values reported are the diffusible content at room temperature. The cross-sectional areas of the beads were measured enabling the hydrogen level to be expressed in terms of fused metal as well as deposited metal. The increase in hydrogen content resulting from exposing basic electrodes at 90% relative humidity is shown plotted for deposited and fused metal in Figure 8. Hydrogen content expressed in terms of deposited metal is used for classification of covered electrodes while hydrogen concentrations reported on the basis of fused metal is reserved for the intercomparison of different welding processes or for use in selecting welding procedures[11].

3.2.1 Hydrogen Diffusion Model

For all steels the critical preheat to avoid cracking was significantly lowered by using low hydrogen (E7018) electrodes instead of cellulosic (E6010) electrodes. The exposure of E7018 electrodes to high humidity for even short times results in a significant increase in hydrogen and an

increase in the preheat required to avoid cracking.

The development of a model for the effects of preheat, hydrogen and chemical composition on cracking has been discussed elsewhere[12]. The main assumption behind the model is that cracking occurs if the average hydrogen concentration remaining in the weld after it cools to 50°C exceeds a critical value which is dependent upon composition. The only effect of preheat is to increase the length of time for the weld to cool to 50°C, which in turn affects the hydrogen content.

The mean hydrogen concentration remaining in a solid after time t is approximately given by

$$\overline{C} = \overline{C}_o A \exp(-\beta_o Dt) \qquad (1)$$

where $\overline{C}_o$ is the original mean hydrogen concentration, D is the diffusion coefficient, and A and β_o are constants that depend on geometry and boundary conditions. To account for the variation in diffusion coefficient with time, the term Dt is replaced by

$$\tau = \Sigma_i D_i \Delta t_i$$

where D_i is the diffusion coefficient at the average temperature T_i where the solid remains for the interval of time Δt_i. The time intervals have been measured from cooling curves for G-BOP tests and the calculation of τ is shown in Table 3. A plot of τ against temperature difference,

θ, is given in Figure 9. Repeat measurements of τ for θ = 78, 128 and 178°C are not shown in the calculations but the values appear in Figure 9.

Assuming that the critical mean hydrogen concentration to produce cracking (below 50°C) is a function of composition and if the critical preheat to give zero cracking is that which allows the original hydrogen content to be reduced to the critical value at 50°C then equation (1) may be rewritten as:-

$$\log_{10} (H_f) + f(\text{composition}) = \beta\tau_c \qquad (2)$$

where $\beta = \beta_o/2.3$ and, τ_c corresponds to θ_c to give zero cracking. The value of β can be found by plotting $\log_{10}(H_f)$ vs. τ_c for one composition. This has been done for steel 133 using four different hydrogen levels and shown in Figure 10. The value of β taken from the slope of the line is $\beta = 60\ cm^{-2}$. Equation (2) can then be rearranged to read:-

$$\beta\tau_c - \log_{10}(H_f) = f(\text{composition}) \qquad (3)$$

where a suitable function of composition is to be determined.

3.2.2 Effects of Composition

In previous work[12] on cracking tests using regular carbon steels, a simple linear relationship using a conventional carbon equivalent formula

for f(composition) in eq'n (3) gave good results and was first examined here to interpret the cracking susceptibility. No significant correlation between the cracking tendency ($\beta\tau_c - \log_{10}H_f$) and composition expressed by using a CE formula was observed. The CE relationship had been developed as a means to predict hardenability and HAZ cracking susceptibility for carbon steels, and there is no basis for assuming that the formula may be applied to weld metals, let alone to HSLA steels. The conventional CE neglects the contribution of alloying elements that promote hardenability in low alloy steels such as niobium and vanadium. A review[13] of existing formulae had shown that the weldability of HSLA pipeline steels is best expressed using the Ito and Bessyo (2) cracking index P_{cm} (a). Its relationship against $\beta\tau_c - \log_{10}(H_f)$ was ar improvement over using CE in the present works. From the G-BOP tests it was shown that Nb significantly increased the preheat required to avoid cracking so that Nb content should be included into a crack susceptibility parameter. The effect of Nb can be estimated by comparing the weld metal compositions of alloys 132 and 136, which are essentially similar except for 0.06 wt.% Nb in the latter. The shift in the crack/no-crack boundary for $\beta\tau_c$ vs f(composition) + $\log_{10}(H_f)$ due to .06 wt. % Nb is equivalent to 0.8 wt % C and thus a multiplying factor of 1.3 is used to describe the effect of Nb. This effect is included in the P_{cm} values in Figure 11.

The effect of composition is difficult to ascertain from Figure 11 because the small range of compositions do not exhibit a linear relationship which

---

(a) $P_{cm} = C + \frac{Mn}{20} + \frac{Si}{30} + \frac{Ni}{60} + \frac{Mo}{15} + \frac{V}{10}$

would be easy to extend over wider compositional variations. A sufficiently large range of chemical compositions to accurately determine the dependence of the cracking tendency on the weld metal chemistry was not covered by the present program.

A possible relationship between chemical composition and degree of cracking for the G-BOP test with cellulosic electrodes was examined using an analysis of variance (ANOVA) with chemical composition and preheat as the variables. Details of the calculation procedure are given in Appendix C. A two-way ANOVA indicated that both chemical composition and preheat significantly affect the results. The effect of preheat on crack susceptibility was anticipated and confirmed by the ANOVA. Although the ANOVA was able to confirm that the cracking behaviour depended on the chemical composition, it was not able to specify which microalloy additions are the most detrimental. A variation of the ANOVA test was able to show which heats were significantly different. The method used was to remove the results for one or more alloys at a time from the cracking results and perform an ANOVA on the remaining heats. Using this approach it was found that by removing the results of 136 and 139 there was no significant effect of composition. In other words, the results for all of the alloys besides 136 and 139 could be considered not significantly different. These two steels were the only alloys containing niobium indicating that Nb tends to promote hydrogen induced cracking of weld metal.

The preheat required to avoid weld metal cracking was lowered by Mn additions (see Figure 12). A 0.3 wt. % increase in Mn lowered the preheat by 20°C. There was also a corresponding increase in hardness which is consistent with the effect of Mn on hardenability. In order to confirm this effect an ANOVA was done on the cracking results for welds whose compositions were similar except for increases in Mn (134, 132, 135), but from the results it was not possible to conclude whether the effect of manganese was significant at a 10% level even though Figure 12 appears to show a beneficial effect.

Mn additions in HSLA steels have been reported to improve the toughness as determined by Charpy impact testing[14]. The effect is attributed to the formation of low temperature transformation products such as acicular ferrite with increasing Mn content[14,15]. A large volume fraction of acicular ferrite is generally considered to improve fracture toughness for low-alloy weld metals. Extending this argument to weld metal cracking due to H_2 embrittlement, the beneficial shift in preheat temperature can be argued to result from an increase in acicular ferrite content. However, microstructural studies are required to verify this postulate.

3.3 Heat-Affected Zone Cracking Tests

Because difficulties were encountered in producing cracking in all steels at one level of applied stress, the implants were artificially strengthened by quenching from austenite. The results of these implant

tests, which were torqued to produce a uniaxial stress of 420 N/mm^2, are listed in Table 4. A preheat of 28°C eliminated cracking in all but three alloys: 133, 135, and 138; compared to the base chemistry of 0.1 C - 1.0 Mn, these steels have slightly higher values of C, Mn and Mo, respectively. Preheating to 60°C above ambient temperatures eliminated the cracking in these alloys.

The detrimental effects of C and Mn on HAZ cracking are well known, and Mo has been found to reduce HAZ toughness in some [16], but not all, cases. The other elements studied (Nb, V, and Ni) do not promote HAZ cracking and this is substantiated in the limited results presented here.

A report on conventional implant tests of HSLA steels[17] does not indicate a significant correlation between the lower critical stress and the HAZ hardness. Maximum hardness, hydrogen content, and microstructure are generally considered to be the primary factors which control the crack susceptibility of the HAZ. Hardenability in high strength steels is obtained through precipitation hardening and control of transformation products, with very little martensite formed. Compared to plain carbon steels, HSLA materials may produce similar HAZ hardnesses, but with considerably less martensite. Martensite laths have been observed to promote cracking because of the diffusion of hydrogen towards dislocations on slip planes which are abundant in martensitic structures[18]. Since the volume fraction of martensite is low the effect of hardness and the relationship to HAZ cracking does not necessarily relate to microstructure in HSLA steels. Therefore, metallographic studies are required to determine the mechanism of hydrogen-assisted cracking in low carbon steels,

in which the hardness is controlled by microalloying elements.

The modified implant test has given promising results as a method of predicting cold cracking in the HAZ resulting from hydrogen embrittlement. The inconsistent cracking behaviour of the modified implants may be eliminated when the test is applied to higher carbon materials, since even conventional implants have been unreliable on HSLA materials.

3.4 Y-Groove High Restraint Cracking Tests

The configuration of this test was chosen to simulate an actual weld joint at a level of restraint which would promote cracking. The restraint length, 1 (see Figure 4), was chosen to be 25mm. Preliminary tests using greater restraint lengths did not promote cracks at room temperature. The restraint length is used to calculate the intensity of restraint, K, as in the following section. The intensity of restraint "represents the reaction force per unit weld length necessary to produce an average elastic change of unit magnitude in the root gap along the weld line[19]."

The results of these tests are shown in Figure 13 and Appendix D. Each steel was welded at a minimum of four preheat temperatures to determine the critical preheat temperature above which cracking will not occur. As with the G-BOP and implant tests, the intersection on the abscissa of a line with a slope of -2 is used to specify a critical preheat. To

differentiate this critical preheat from that for G-BOP tests it will be given as θ_{CHR}, critical preheat for high restraint. The values of the integrated diffusion coefficient for the high restraint tests, τ_{CHR} which correspond to θ_{CHR} can be read directly from Figure 9. The curves for the crack sensitivity in the weld cross-section (the value A in Figure 5) are used to determine the values of θ_{CHR}. These preheats, as well as the hardnesses are listed in Table 5. The maximum HAZ hardnesses increase with greater values of CE or P_{cm} but there is no relationship between the hardness and critical preheats nor between the hardenability indexes (CE, P_{cm}) and the critical preheats. This will be discussed further in section 3.4.2.

3.4.1 Intensity of Restraint

The final reaction stress in a weld depends upon the shape of the weld bead and the restraining forces across the weld. The relationship is determined by:

$$(\sigma_w)_{t\to\infty} = mK \qquad (4)$$

where m = a numerical factor that depends upon the electrode and bevel angle = 0.038[19]

K = intensity of restraint = $\frac{Eh}{\ell}$

E = Young's modulus, 210 kN/mm^2

h = plate thickness, mm

ℓ = restraint length, mm

Since the value of m is a constant, the reaction stress is determined uniquely by the intensity of restraint. Although all the plates were not the same thickness, the intensity of restraint did not affect the results because the stress as calculated by equation (4) was well above yield in all cases. It has been shown in Tekken tests that the intensity of restraint does not exceed 28000 N/mm^2 (20). In the same report Suzuki also states that the bevel groove used in the present results can be considered to behave similarly to the sloping groove in a Tekken test so that the maximum value should be taken as $K = 28000\ N/mm^2$ and $\sigma_w = 1064\ N/mm^2$, which is considerably above yield.

The intensity of restraint is therefore at its maximum value and the reaction stress is sufficient to produce cracking.

3.4.2 Chemical Composition

The results of the cracking tests in Figure 13 can be used to estimate the relative crack susceptibility of the steels as compared to the high carbon material 13A. Steels 13B, 13C, 13D and 13F have similar crack sensitivities to 13A as measured in Figure 13 (a) using the method outlined in section 3.2 but 13C and 13D are more susceptible to root cracking than 13A (Figure 13(b)). Only steel 13E had considerably lower crack sensitivities, and it was the only composition which did not contain microalloying elements.

In section 3.2.2 the parameter P_{cm}, which included an effect due to niobium, was used to examine cracking tests. It was proposed that a dependence exists between $\beta\tau_c - \log_{10}(H_f)$ and P_{cm}. However, in order to establish a correlation between these variables, a value of β for the high restraint tests to be calculated. Using the results for steel 13A at low and high hydrogen conditions a value of $\beta = 140\ cm^{-2}$ was determined for these tests. As with the G-BOP tests, the cooling rates were monitored for these restraint welds in order to obtain the integrated diffusion coefficient, τ(see Figure 9). Although they lie close to the G-BOP values, a separate curve is shown since uncertainties exist for θ greater than $120^{o}C$. The values for $\beta\tau_c - \log_{10}(H_f)$ are plotted against P_{cm} with the earlier results in Figure 11. Apart from the results for 13A and 13C the remaining results seem to agree with the G-BOP results. This result is significant because it indicates that small, inexpensive tests such as the G-BOP may be applied to actual weld configurations to predict cracking, providing that joint geometries are considered.

An interesting observations in Figure 13(a) is that the slope of curve 13C is less than the others. A possible explanation is that the maximum HAZ hardness for steel 13C is almost insensitive to preheat so that cracks initiate at the root of the weld. It has been observed in these cross-sections that cracks usually start at the WM/HAZ interface, and thus, the hardness of this region is important when considering crack susceptibility.

The initiation of hydrogen cracks appears to depend on the hardness of the HAZ, but the controlling factor for crack propagation is still unknown. During metallographic examinations for the presence of cracks, the actual paths and dimensions were recorded, with particular emphasis as to whether the crack propagated through the weld or HAZ. In all but steel 13B, the crack ran mainly through the weld metal. The welds without preheat are shown in Figure 14 for steels 13B, 13C, and 13D, showing the actual crack path at mid-length. In these sections it appears that increasing the niobium content shifts the crack propagation path to the weld metal from the heat-affected zone. Therefore, in alloys with large amounts of niobium, dilution into the weld may increase the crack susceptibility of the weld which may in some way be due to easier crack propagation in the presence of niobium.

3.5 Instrumented Restraint Cracking Tests

Small-scale restraint tests were conducted to determine whether the weld metal or the heat-affected zone controlled hydrogen cracking in HSLA steels. The present series of tests using strain gauge restraint arms was conducted primarily to quantify the restraint stress across the root weld in a bevel groove. The actual reaction forces could then be compared to calculated values to see whether reaction stresses in root welds can be predicted so that estimates of crack susceptibility of different weld configurations can be calculated.

It was anticipated that the high-restraint tests would crack at room temperature while the low-restraint tests would not. A critical preheat to avoid cracking for known restraint levels could then be determined. However, cracks were not observed and therefore only the reaction force information was obtained as a function of temperature and composition.

3.5.1 Measurement of Reaction Forces

The reaction force across the weld may be calculated using equation (4) in which the intensity of restraint is considered to be a parallel combination of the restraint in the sidearms and in the test section.

low restraint:

restraint in sidearms = $K_s = \frac{Eh}{\ell} = \frac{210000}{250} \times 50 = 42000 \ \frac{N}{mm^2}$

restraint across weld = $K_w = \frac{Eh}{\ell} = \frac{210000}{250} \times 14 = 11760 \ \frac{N}{mm^2}$ for 13D

$K_w = \frac{Eh}{\ell} = \frac{210000}{250} \times 19 = 15120 \ \frac{N}{mm^2}$ for remaining compositions

total nominal restraint = $\frac{1}{K_T} = \frac{1}{K_s} + \frac{1}{K_w}$

$K_T = 9200 \ N/mm^2$ for 13D

$K_T = 11120 \ N/mm^2$ for remaining compositions

high restraint:

$K_S = 7000\ N/mm^2$

$K_w = 19600\ N/mm^2$ for 13D

$K_w = 25200\ N/mm^2$ for remaining compositions

$K_T = 15300\ N/mm^2$ for 13D

$K_T = 18500\ N/mm^2$ for remaining compositions

The limiting value of the reaction stress occurs when the weld metal yields (which is approximately 500 N/mm^2) and this corresponds to a minimum level of restraint of $K = \sigma/m = 500/0.038 = 13160\ N/mm^2$. Therefore, based on these calculations, the low restraint tests should not yield, whereas the high restraint tests should yield across the weld and produce cracks.

The stress is calculated from the strains measured in the sidearms. The total area of the sidearms was chosen to approximate the area of the test piece so that the strains would be similar.

The calculated strains for the low and high restraint conditions across the weld are approximately 433 $\mu\varepsilon$ and 610 $\mu\varepsilon$, respectively.

The development of the reaction force in relation to the time after start of welding for the high restraint tests are shown in Figures 15a), b), and c) for $\theta = 0$, 60, and 100 C^o, respectively. The values in Figure 15 are averages for each reaction arm, the total force being

double the average. Also included in Figure 15 is the temperature of the baseplate adjacent to the weld which shows the relationship between the thermal cycle and reaction force. The reaction force begins to develop shortly after the weld is completed and increases rapidly within the next 15 minutes. The force then levels off to a value close to the final value. The results of the reaction force measurements for the low restraint tests are shown in Figure 15 (d). The forces increase shortly after welding has been completed, as in the high restraint tests. The final reaction stress is lower for these tests as expected compared to the high restraint condition.

The relationship between calculated and measured values of the reaction forces are presented in Figure 16. In all cases the actual restraint force was less than the predicted value. This may be attributed to a number of factors. The expected restraint forces are calculated assuming that yielding occurs in the weld metal but examination of these welds at several cross-sections did not reveal any cracking. Therefore the reaction stresses were not sufficient to crack the welds as anticipated. Effects of bending are also likely to reduce the reaction forces. Bending both in the plane of the plate and also through the thickness has been examined in H-tests [21] which are similar to the instrumented tests except that the reaction arms are not the same thickness as the test material. It was reported[21] that the top surface may be in tension while the bottom is in compression. This would result in considerable rotation about the actual weld and thus lower the reaction forces, which may be responsible for the difference noted here.

The tests performed at various temperatures should have exhibited the same reaction forces and the only variable should have been the resultant weld metal hydrogen level. However, the results in Figure 15 indicate that differences are observed which depend upon the test temperature. The variations are due to minor unavoidable effects of misalignment since the temperature effects were prevented by preheating the complete test assembly and using a temperature compensating bridge configuration to measure the reaction strains. The tests conducted at 60°C above room temperature are considered to be the most representative (i.e. neglibible misalignment) since the strain did not change from the preload value as the assembly was heated. The average reaction force appears to lie between 30 and 35 kN for the high restraint tests while the expected values were between 100 and 110 kN. The one third difference agrees with previous work on lamellar tearing[21] and is mainly due to bending within the test assembly. The test configuration used in the present program was modified to hopefully reduce some of the bending associated with H-tests[21], but it appears that the same effects were observed.

These effects resulted from small misalignments before welding, and bending after welding due to the complex stress distribution along the weld and also through the thickness. Although the reaction stresses were insufficient to promote cracking it was found that preheating did not change the final reaction forces once the weld had cooled to room temperature. Since cracking did not occur in these tests it was not possible to determine a relationship between hydrogen content, composition, and restraint.

4. CONCLUSIONS

The main results obtained in this program can be summarized as follows:

1. The results of the G-BOP tests have shown that niobium diluted from the base metal increases the crack susceptibility of the weld metal while manganese reduces the amount of cracking.

2. Cold cracking in HSLA steels depends on the concentration of hydrogen remaining in the vicinity of the weld after it has cooled down to ambient temperatures. The logarithm of the hydrogen concentration is related to the amount of cracking as affected by preheat.

3. The relationship between alloying and the amount of cracking as measured in the G-BOP test can be related by using P_{cm} as the susceptibility index instead of a conventional carbon equivalent. A term 1.3 Nb should be included in the P_{cm} index to include the effect of niobium.

4. The modified implant test developed in this program is an inexpensive means to test the susceptibility of the HAZ to hydrogen cracking. The improved crack resistance of HSLA steels in the heat-affected zone and the large differences in strengths between steels which affect the results of conventional implant tests are not significant in the modified implant test, since a preheat temperature and not strength is the result obtained from the latter test.

5. The high restraint tests also confirmed the detrimental effect that niobium has upon hydrogen cracking.

6. Measured reaction forces in instrumented restraint tests are lower than predicted values because of problems encountered with proper alignment of the test specimens before welding and non-uniform shrinkage after the weld has been completed.

ssm

REFERENCES

1. Pickering, F.B., High-Strength, Low Alloy Steels - A Decade of Progress, Microalloying 75 Proceedings, Union Carbide Corp., New York, N.Y. 1977, p.9.

2. Ito, Y. & Bessyo, K., Weldability Formula of High Strength Steels, IIW Doc. No. IX-576-68

3. Kerr, H.W., A Review of Factors Affecting Toughness in Welded Steels, Int. J. Pres. Ves. & Piping, 4 (1976), p.119.

4. Graville, B.A., & McParlan, M., Weld Metal Cold Cracking, Metal Construction and British Welding Journal, 6 (1974), p.62.

5. McParlan, M. & Graville, B.A., Development of the G-BOP test for Weld Metal Cracking, IIW Doc. No. IX - 922-75.

6. Welding-Determination of Hydrogen in Deposited Weld Metal Arising from the Use of Covered Electrodes for Welding Mild and Low Alloy Steels, ISO Standard 3690-1977(E).

7. Kihara, H., Terai, K., Yamada, S., Nogano, T., Study on Preheating Temperatures in Welds of High Strength Steel Structure, IIW Doc. No. IX-677-70.

8. Glover, A.G., Compositional Characterization of Hydrogen Cracking in Line Pipe Materials, Welding Institute of Canada Report PR-140-105, June 1980.

9. Lazor, R.B., Structure Property Relationships in HSLA Weld Metal, M.A. Sc. Thesis, University of Waterloo, Waterloo, Ontario 1979.

10. Sawhill, J.M.Jr., Climax Molybdenum Co. Report ISJ-786, August 1973.

11. Recommended Methods of Reporting Single Bead Weld Metal Hydrogen Contents, Doc. IIS/IIW-532-77.

12. McParlan, M. & Graville, B.A., Hydrogen Cracking in Weld Metals, Welding Journal, 55(1976), p. 95-s.

13. Bersch, B. & Koch, F.D., Weldability Estimation of HSLA-Pipeline Steels, IIW Doc. No. XI-E-4-80, May 1980

14. Widgery, D.J., Deoxidation Practice for Mild Steel Weld Metal, Welding Journal, 55(1976), p.57-s.

15. Ito, Y. & Nakanishi, M., Study on Charpy Impact Properties of Weld Metal with Submerged-Arc Welding, Sumitomo Search No. 15, May 1976, p.42.

16. Shiga, A., Imura, M., Tsuboi, J., Notch Toughness of Niobium Bearing Steel Weldment, IIW Doc. No. IX-880-74.

17. Bryhan, A.J., Analysis of Implant Test Data, Climax Molybdenum Co. Report L-176-203, Feb 1979.

18. Kikuta, Y., & Araki, T., Microscopic Redistribution Behaviours of Hydrogen and Fracture Morphology of HAZ Cold Cracking in High Strength Steel, IIW Doc. No. IX-1165-80.

19. Satoh, K. & Matsui, S., Reaction Stress and Weld Cracking Under Hindered Contraction, IIW, Doc. No. IX-574-68.

20. Suzuki, H., Cold Cracking and Its Prevention in Steel Welding, IIW Doc. No. IX-1074-78.

21. Malik, L. & Graville, B.A., Effect of Joint Restraint on Lamellar Tearing Susceptibility in Steel Plates, Welding Journal, 58(1979) p.12-s.

ssm

TABLE 1

Composition of Steels and Consumables

Alloy No.	Chemical Composition, wt. %											
	C	Mn	Si	Al	S	P	Ni	Cr	Mo	Nb	V	Other
131	.045	1.45	.25	.04								
132	.11	1.47	.30	.06								
133	.13	1.41	.25	.02								
134	.08	1.05	.28	.04								
135	.11	2.10	.29	.06								
136	.115	1.44	.24	.03						.09		
137	.095	1.60	.29	.04							.11	
138	.11	1.50	.33	.03					.30			
139	.10	1.43	.33	.02					.30	.10		
1310	.09	1.49	.24	.06			1.99					
13A	.22	1.38	.01		.021	.011						
13B	.054	2.09	.13		.005	.016	.23	.07	.34	.031		
13C	.055	2.00	.32		.003	.003	.23	.03	.36	.057		
13D	.06	1.81	.20	.036	.003	.003			.38	.042		
13E	.086	1.15	.22	.06	.013	.006						.0055N
13F	.10	1.33	.25	.04	.011	.005					.125	.019N,Ce
13G	.093	1.26	.27		.013	.010				.07	.05	Ce
13H	.092	1.20	.26		.011	.007				.14		
13I	.077	1.41								.12	<.002	
13J	.085	1.24								<.005	.047	
E6010	.08	.51	.24		.02	.003						
E7018	.08	1.11	.36		.019	.003						

TABLE II

Summary of Results of Weld Metal Cracking Tests

Alloy No.	Chemical Composition, wt % C	Mn	Si	Other	Base Metal Hardness DPH_{30}	Weld Metal Hardness DPH_{30}	H_2 Content ml/100 g Metal Dep	Fused	Preheat for zero Cracking θ, °C	CE[b]	P_{cm}[c]	$\beta\tau_c - \log_{10}(H_f)$
131	0.07	0.88	N.A.[a]		130	216	91.2	29.5	108	.217	.123	-.74
							12.3	7.4	18			-.6
132	0.11	1.03	N.A.		160	252	91.2	29.5	98	.282	.171	-.64
							12.3	7.4	38			-.75
133	0.13	0.96	0.28		162	264	91.2	29.5	98	.29	.187	-.74
							12.3	7.4	18			-.75
							17.7	10.1	48			-.75
							32.5	20.0	68			-1.1
134	0.09	0.76	N.A.		161	244	91.2	29.5	118	.217	.137	-.4
							12.3	7.4	<0			
135	0.10	1.33	N.A.		165	263	91.2	29.5	78	.322	.176	-1.0
							12.3	7.4	<0			
136	0.11	0.84	N.A.	0.06Nb	183	256	91.2	29.5	138	.267	.244	-.41
							12.3	7.4	68			0.1
137	0.11	1.06	N.A.	0.05V	185	252	91.2	29.5	108	.287	.177	-.69
							12.3	7.4	28			-.6
138	0.11	1.05	N.A.	0.20Mo	164	259	91.2	29.5	108	.335	.185	-.69
							12.3	7.4	28			-.6
139	0.11	0.96	N.A.	0.06Nb 0.20Mo	210	288	91.2	29.5	128	.27	.266	-.57
							12.3	7.4	48			-.17
1310	0.11	0.97	N.A.	1.21Ni	194	274	91.2	29.5	108	.352	.188	-.64
							12.3	7.4	38			-.6

(a) not analyzed

(b) $CE = .C + \frac{Mn}{6} + \frac{Cr + Mo + V}{5} + \frac{Ni}{15}$

(c) $P_{cm} = C + \frac{Mn}{20} + \frac{Si}{30} + \frac{Ni}{60} + \frac{Mo}{15} + \frac{V}{10} + 1.3\,Nb$

TABLE III

Calculation of τ for $\theta^* = 178, 128, 78, 28$ and $0^{\circ}C$

Temperature Range $^{\circ}C$	Diffusion Coefficient D_i, $cm^2 s^{-1}$	178 Δt_i s	178 $D_i \Delta t_i$ cm^2	128 Δt_i s	128 $D_i \Delta t_i$ cm^2	78 Δt_i s	78 $D_i \Delta t_i$ cm^2	28 Δt_i s	28 $D_i \Delta t_i$ cm^2	0 Δt_i s	0 $D_i \Delta t_i$ cm^2
1500–500	1.3×10^{-4}	10.3	13.4×10^{-4}	9.0	11.7×10^{-4}	8.0	10.4×10^{-4}	7.0	9.1×10^{-4}	6.5	8.45×10^{-4}
500–450	1.53	2.1	3.21	1.4	2.14	1.2	1.84	0.8	1.22	0.7	1.07
450–400	1.30	2.9	3.77	2.0	2.6	1.4	1.82	0.9	1.2	0.8	1.04
400–350	1.07	4.6	4.92	2.5	2.7	1.9	2.03	1.3	1.4	1.1	1.2
350–300	8.58×10^{-5}	10.1	8.7	3.8	3.3	2.5	2.15	1.7	1.46	1.4	1.2
300–275	7.55	17.0	12.8	3.0	2.3	2.2	1.7	1.4	1.06	1.0	0.76
275–250	6.75	35.0	23.0	3.5	2.3	1.7	1.12	1.1	0.72	0.8	0.53
250–225	4.67	183.0	85.5	6.0	2.8	3.0	1.4	1.7	0.8	1.3	0.61
225–200	3.09	300.0	92.7	10.4	3.2	4.4	1.36	2.1	0.65	1.5	0.46
200–175	1.95	380.0	74.1	32.2	6.3	6.8	1.33	2.8	0.55	2.0	0.39
175–150	1.16	404.0	46.9	344.0	39.9	16.5	1.91	4.0	0.46	2.5	0.29
150–125	6.47×10^{-6}	615.0	39.8	870.0	56.3	178.0	11.5	6.4	0.41	3.5	0.23
125–100	3.36	810.0	27.22	975.0	32.8	1100.0	36.96	14.2	0.48	5.9	0.2
100–75	1.5	965.0	14.5	1800.0	27.0	1802.0	27.03	89.3	1.34	10.8	0.16
75–50	6.24×10^{-7}	2640.0	16.5	3400.0	21.2	3470.0	21.7	2200.0	13.9	40.0	0.25
$\tau = \Sigma_i D_i \Delta t_i$			467×10^{-4}		216×10^{-4}		124×10^{-4}		34.7×10^{-4}		16.8×10^{-4}

* θ = temperature difference based on $22^{\circ}C$ room temperature

TABLE IV

Implant Cracking Percentage Results

Alloy No.	Preheat Level, θ, °C		
	0	28	60
131	0, 40, 0	0	
132	0, 80, 20	0	
133	10, 20	100	0
134	0, 70, 100	0	
135	60, 100	40	0
136	0, 10, 0	0	
137	0, 100, 40	0	
138	90, 80	100	0
139	10, 100, 100	0	
1310	95, 0, 30	0	

TABLE 5

Summary of Results of Restraint Tests

Alloy No.	Thickness mm	Preheat θ, °C	Hardness, DPH5 Base Metal	Weld Metal	Max. HAZ Hardness	θ_{CHR}, Preheat for zero Cracking, °C	CE_1	P_c	P_{cm}
13A(1)	13	0	154	294	385	<0	.45	.360	.289
		160		242	272				
13A	13	0	154	234	394	66	.45	.360	.289
		40		231	380				
		60		220	345				
		80		219	324				
13B	19	0	244	267	357	52	.49	.272	.233
		100		235	310				
13C	19	0	224	263	362	56	.48	.274	.269
		100		247	348				
13D	14	0	212	261	350	71	.43	.254	.233
		100		228	311				
13E	19	0	125	222	307	41	.27	.231	.151
		80		198	264				
13F	19	0	179	275	350	66	.34	.267	.187
		80		236	316				
13G	19	0	196	246	331		.31	.251	
13H	19	0	196	239	277		.29	.241	
13I	19	0					.31	.236	
13J	19	0					.30	.240	

(1) Denotes steel welded with E7018 electrodes. All other tests used E6010

$$CE_1 = C + \frac{Mn}{6} + \frac{Cr + Mo + V}{5} + \frac{Ni}{15}$$

$$P_c = C + \frac{Si}{30} + \frac{Mn + Cu + Cr}{20} + \frac{Ni}{60} + \frac{Mo}{15} + \frac{V}{10} + 5B + \frac{t,mm}{60} + \frac{H_f\ ml/100g}{60}$$

$$P_{cm} = C + \frac{Mn}{20} + \frac{Si}{30} + \frac{Ni}{60} + \frac{Mo}{15} + \frac{V}{10} + 1.3\ Nb$$

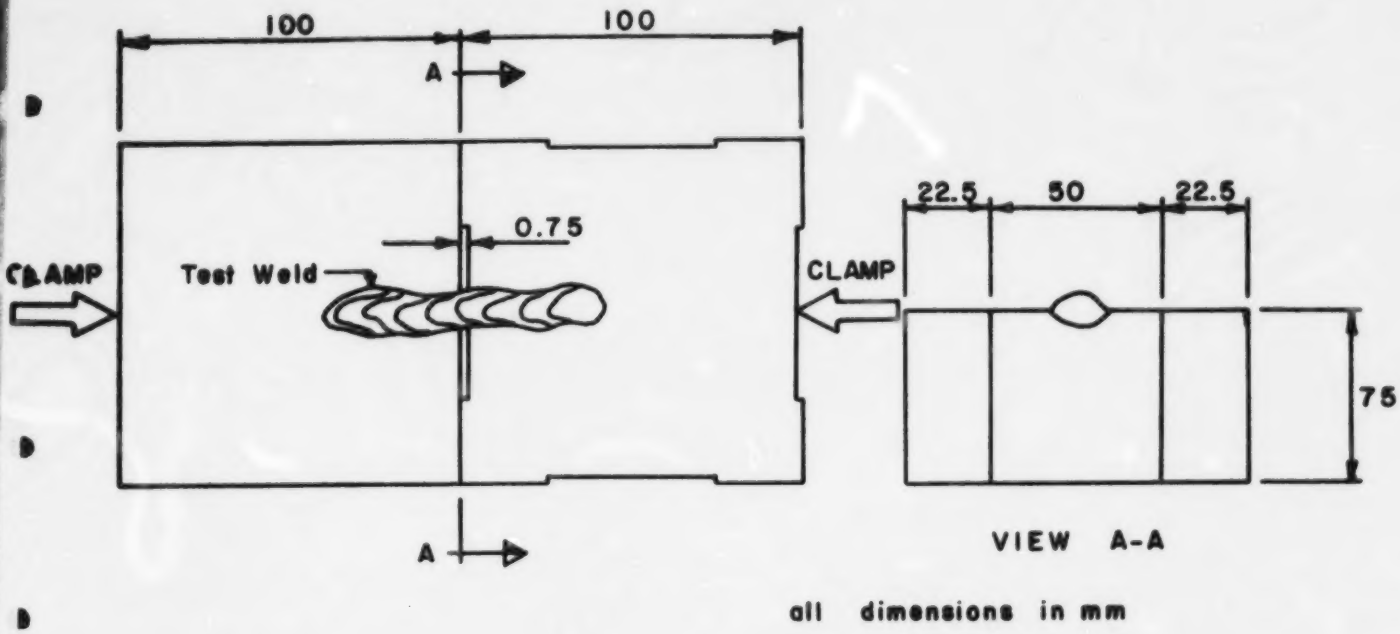

Figure 1: The gapped bead-on-plate (G-BOP) Test

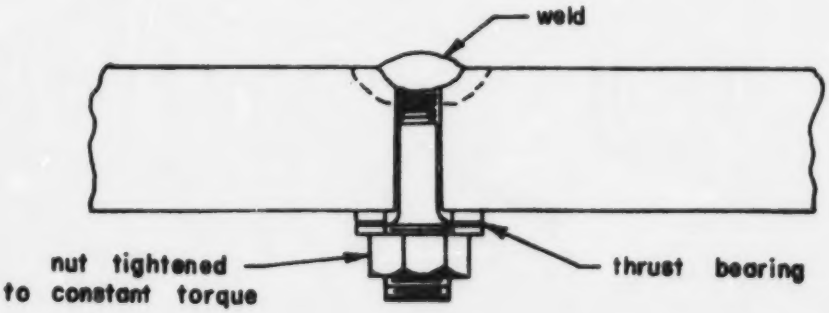

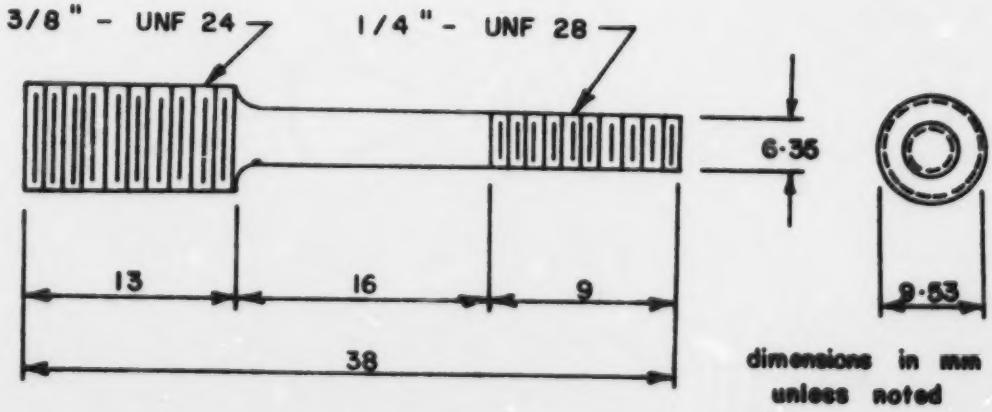

Figure 2: The Modified Implant Test

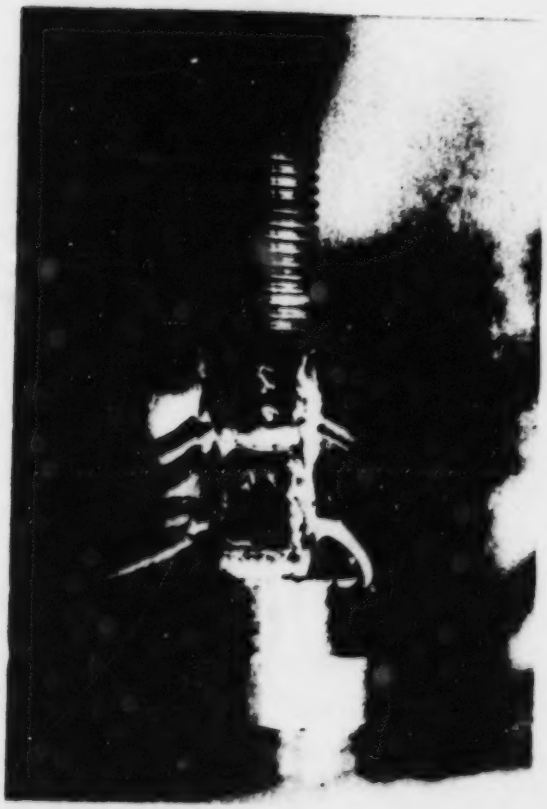

1148

Figure 3: Strain-gauged implant specimen used to calibrate torque vs. stress. Two more strain gauges are located on the other side to complete the bridge (1.6x)

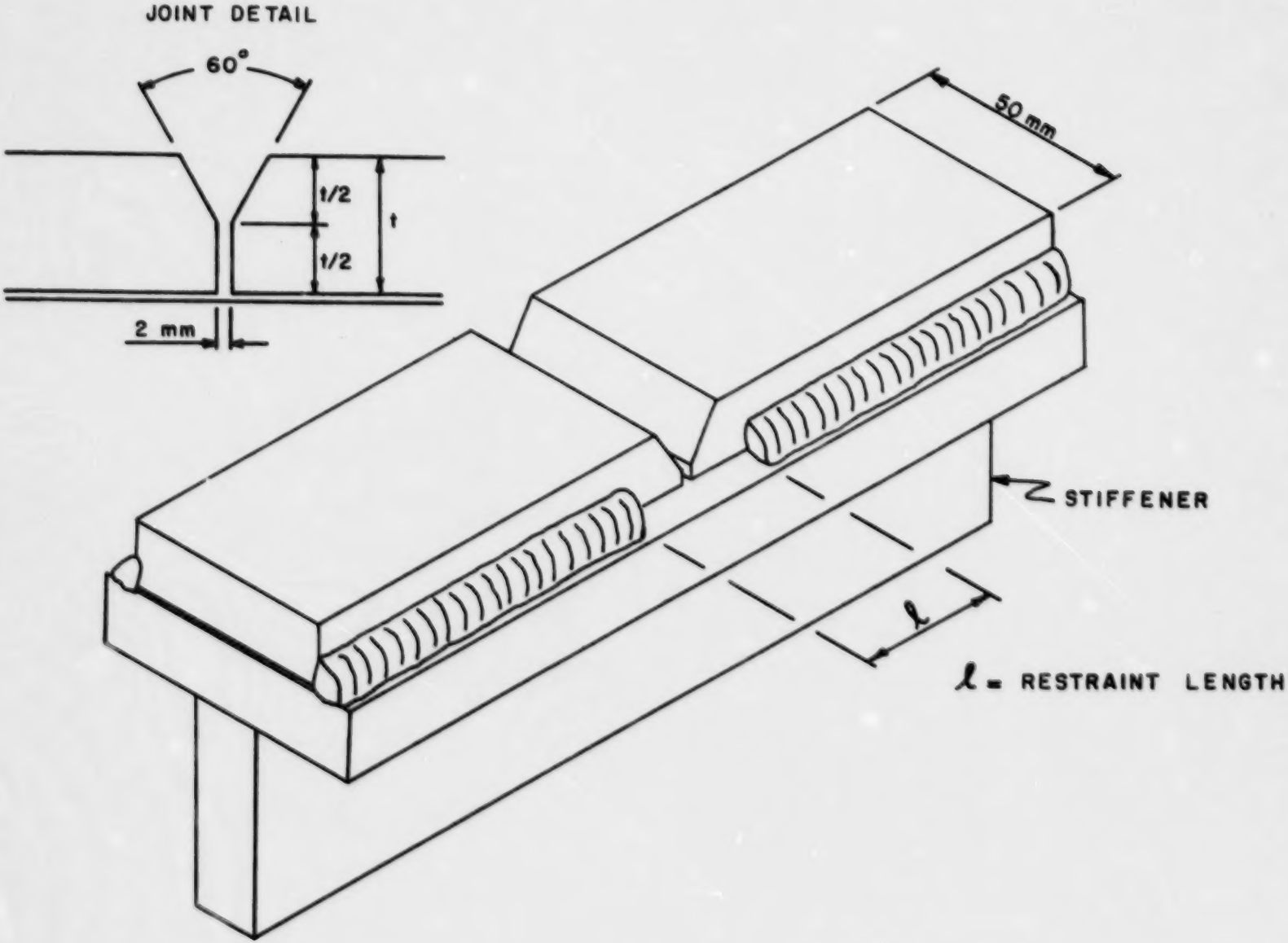

Figure 4: Small scale high restraint cracking test assembly

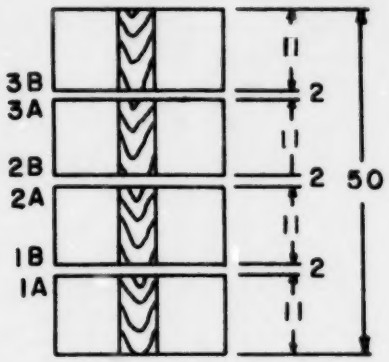

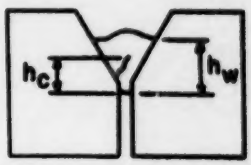

weld cross section

all dimensions in mm

crack sensitivity in cross-section: $A = \frac{1}{6} \Sigma \frac{(h_c)}{h_w} \times 100\%$

crack sensitivity in root : $B = \frac{\text{number of cracked sections}}{6} \times 100\%$

Figure 5: Method of Measuring percentage of cracking in restraint tests (after Kihara et al (1))

115B

Figure 6: Instrumented Restraint Test Assembly Showing Completed Root Weld

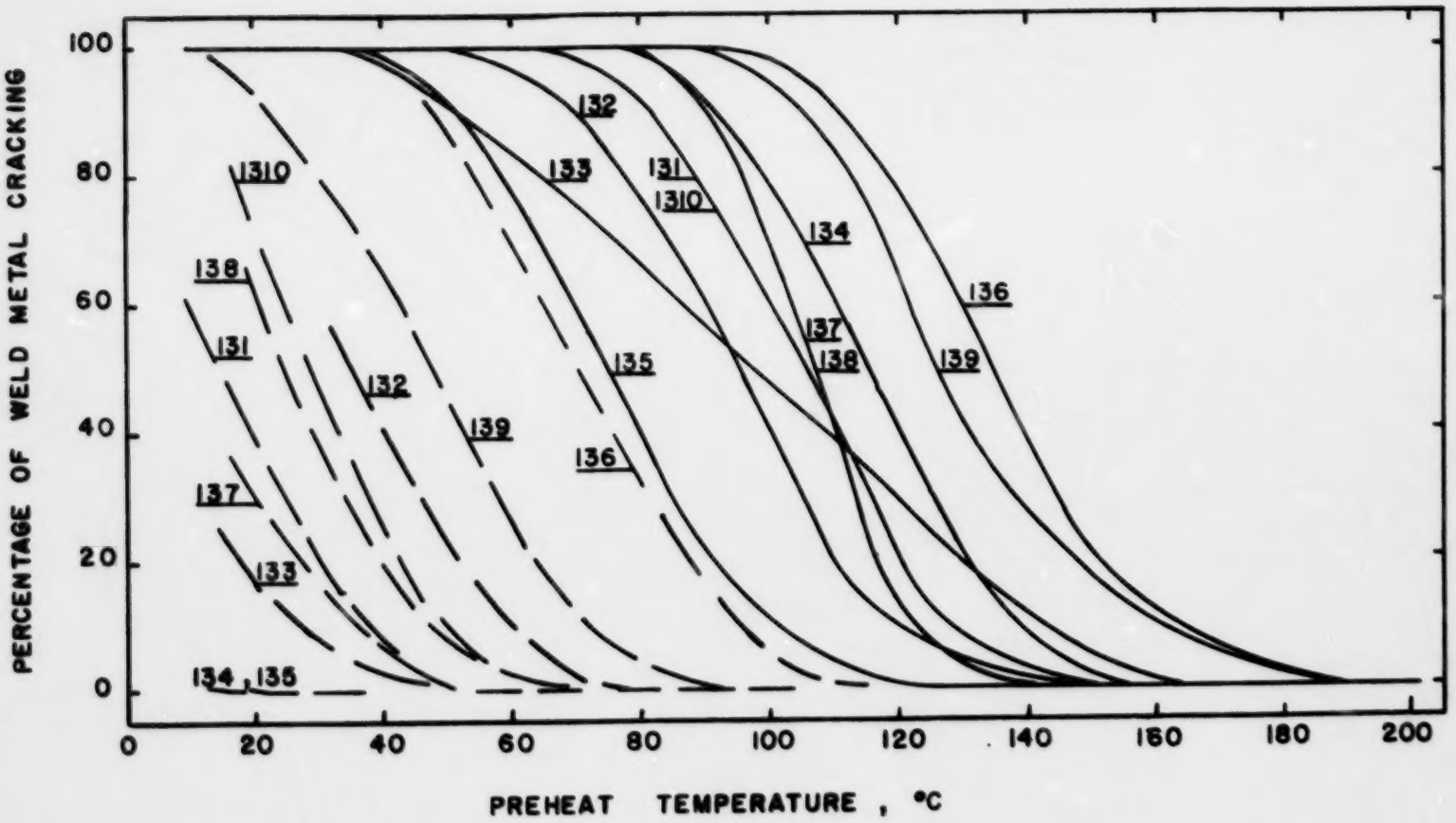

Figure 7: Weld Metal Cracking Percentage vs. preheat temperature from G-BOP tests

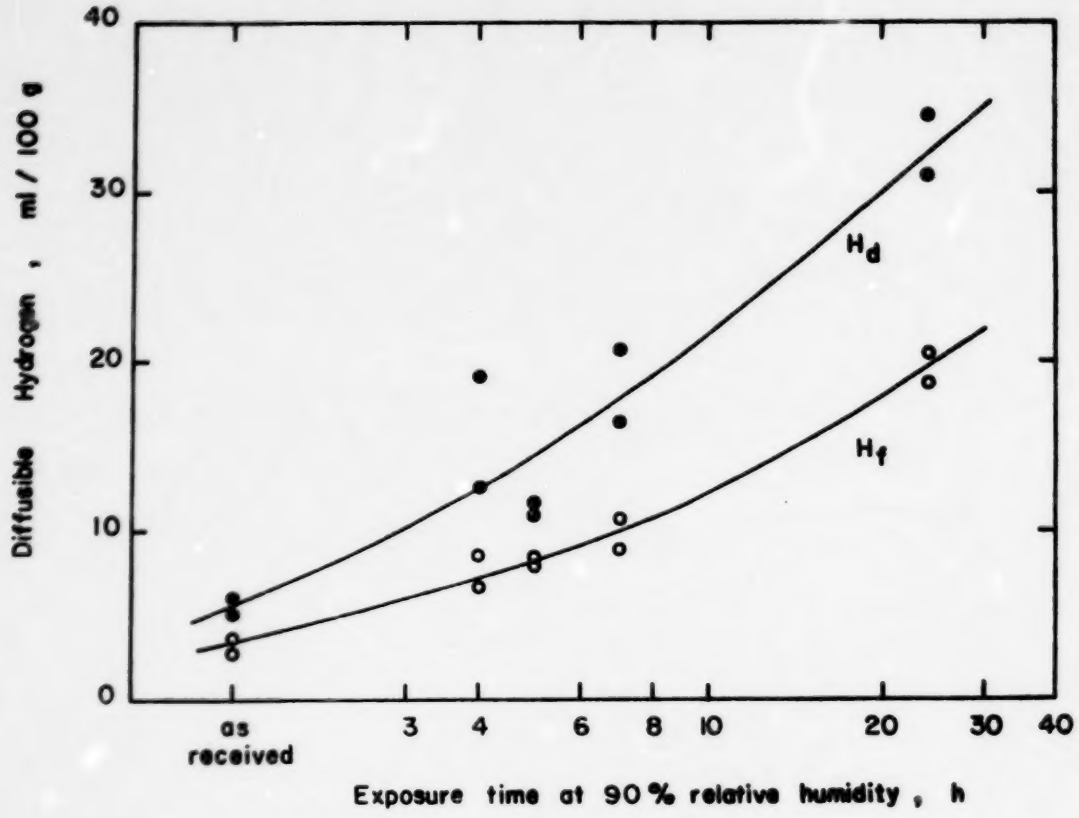

Figure 8: Weld metal hydrogen content vs. exposure time at 90% relative humidity for basic electrodes.

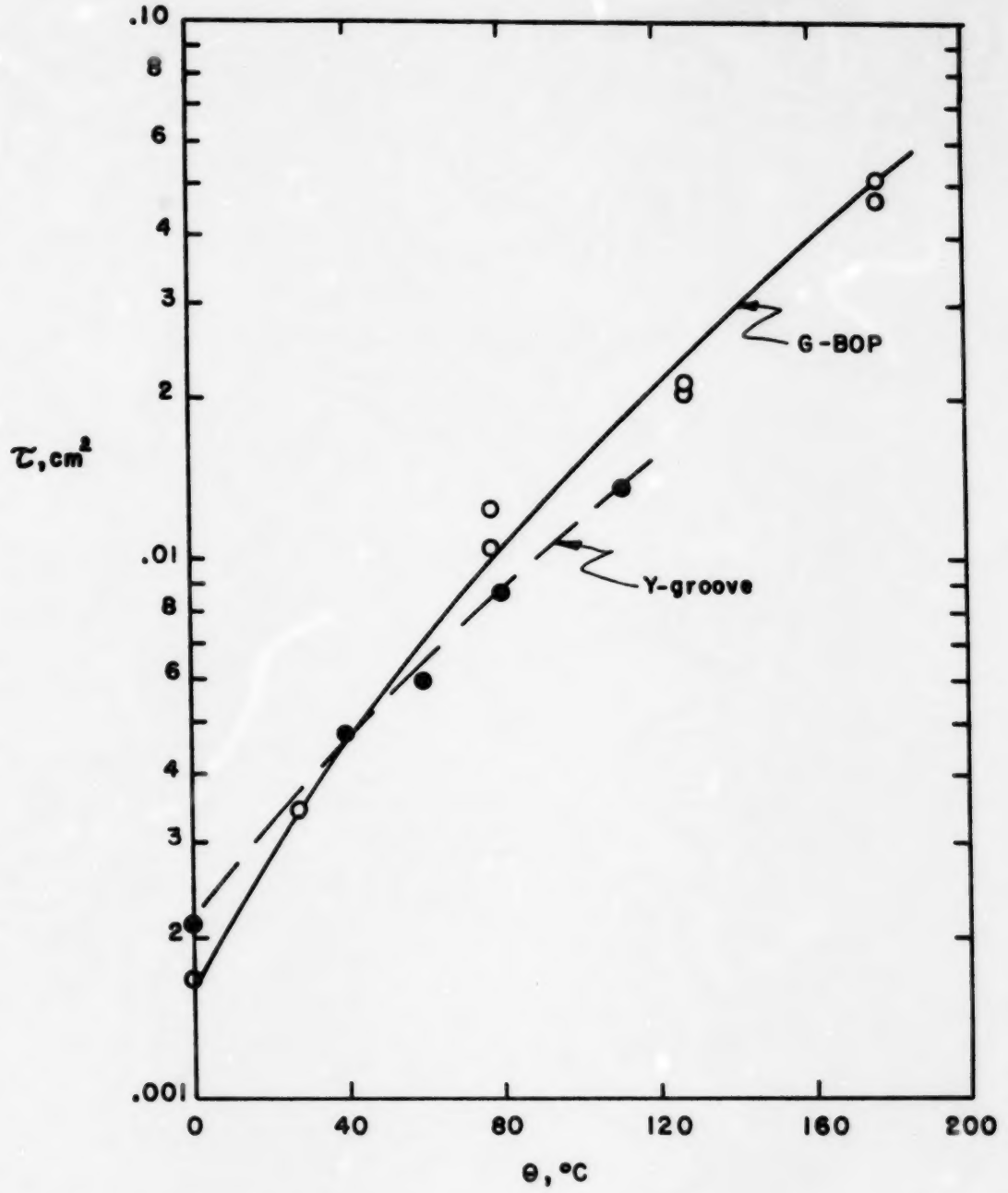

Figure 9: Plot of τ against preheat temperature

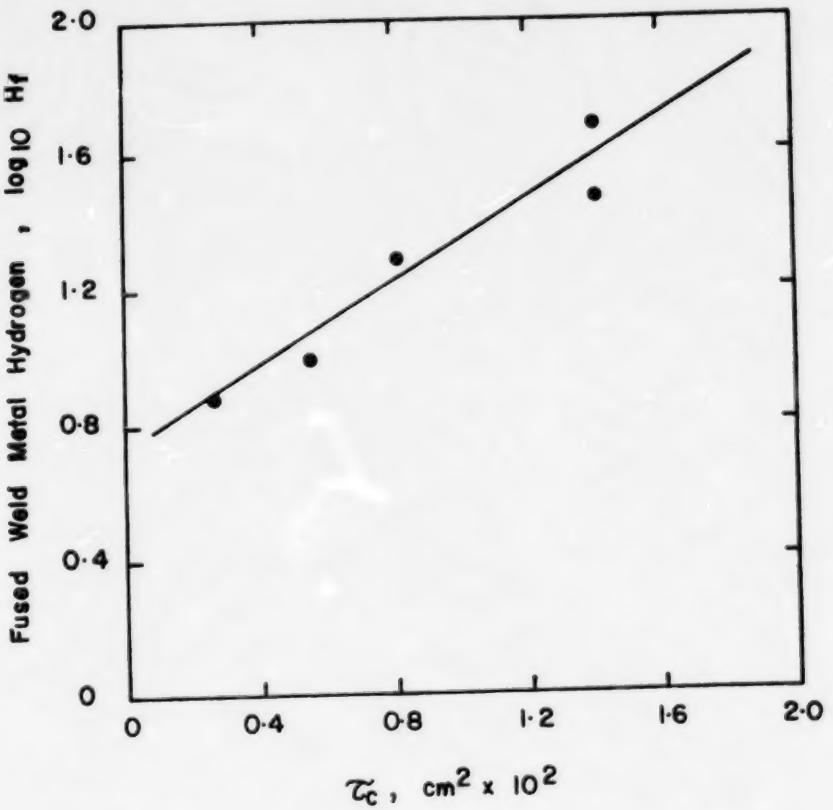

Figure 10: Relationship between $\log_{10}(H_f)$ and τ_c for steel 133.

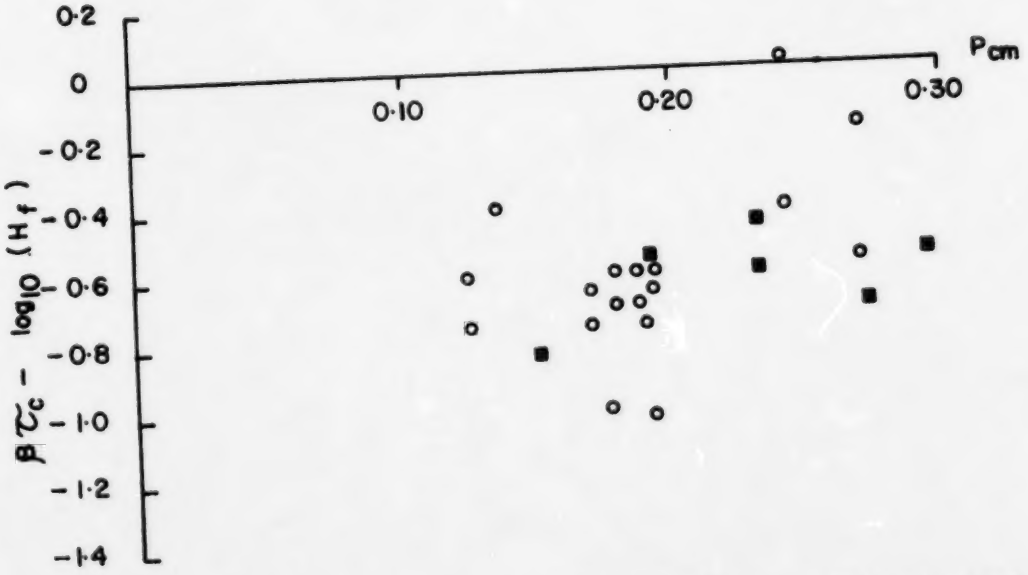

Figure 11: Relationship between $\beta\tau_c - \log_{10}(H_f)$ and chemical composition

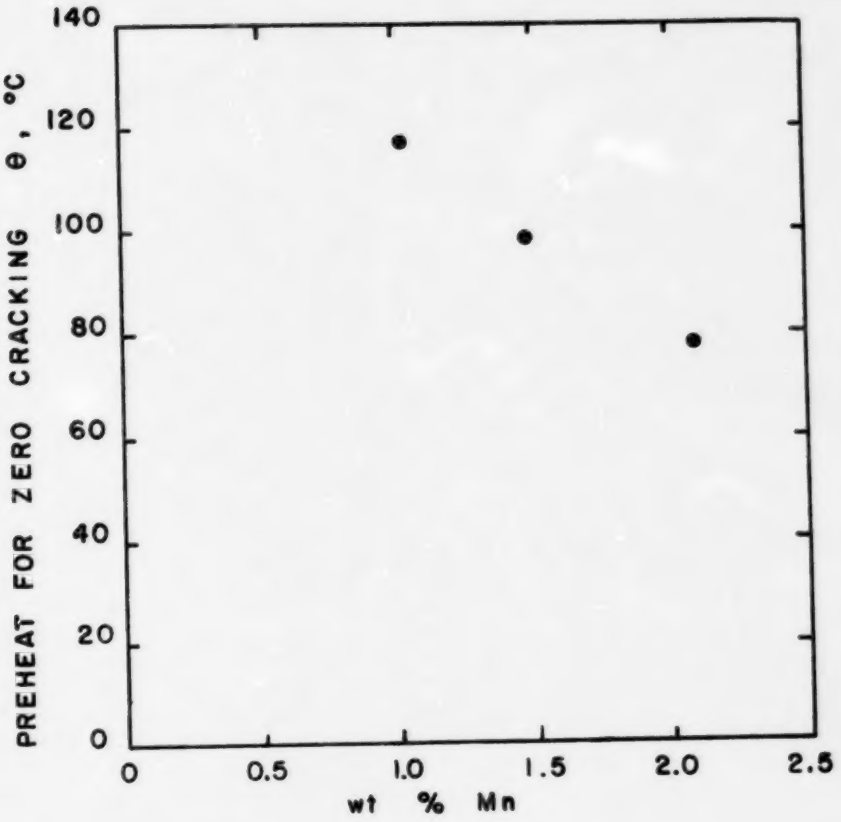

Figure 12: Manganese content vs critical preheat temperature

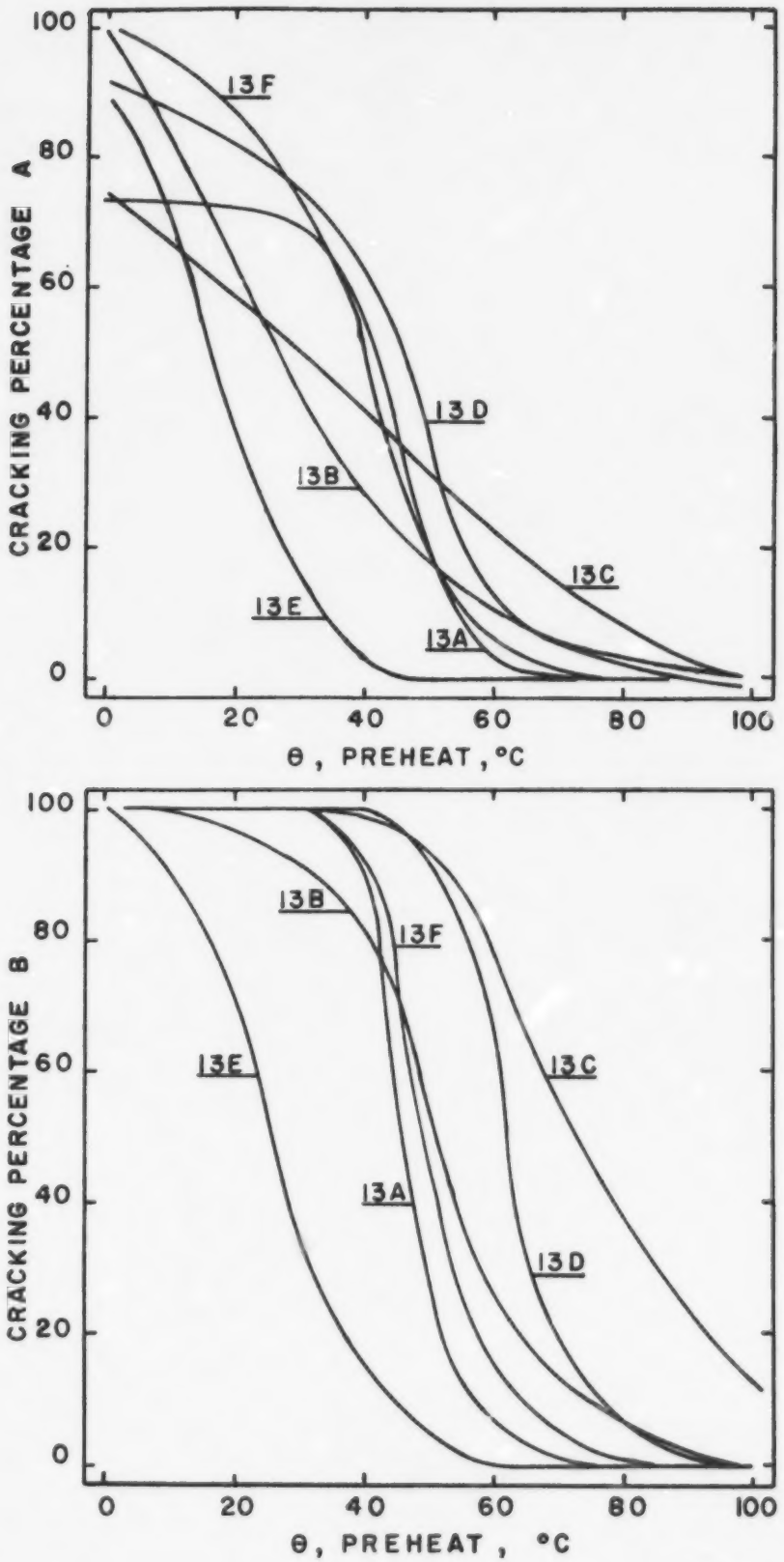

Figure 13 (a) - (above) Cracking Percentage A vs. preheat for high restraint tests

(b) - (below) Crack Sensitivity B vs. preheat for high restraint tests

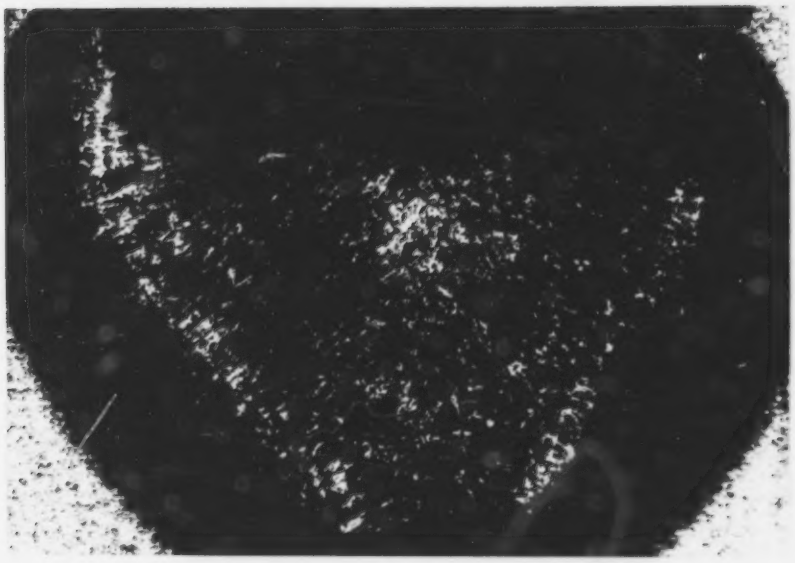

55B

Figure 14 (a): Cross-section of cracked restraint test weld, steel 13B, room temperature

56B

Figure 14 (b): Cross-section of cracked restraint test weld, steel 13C, room temperature

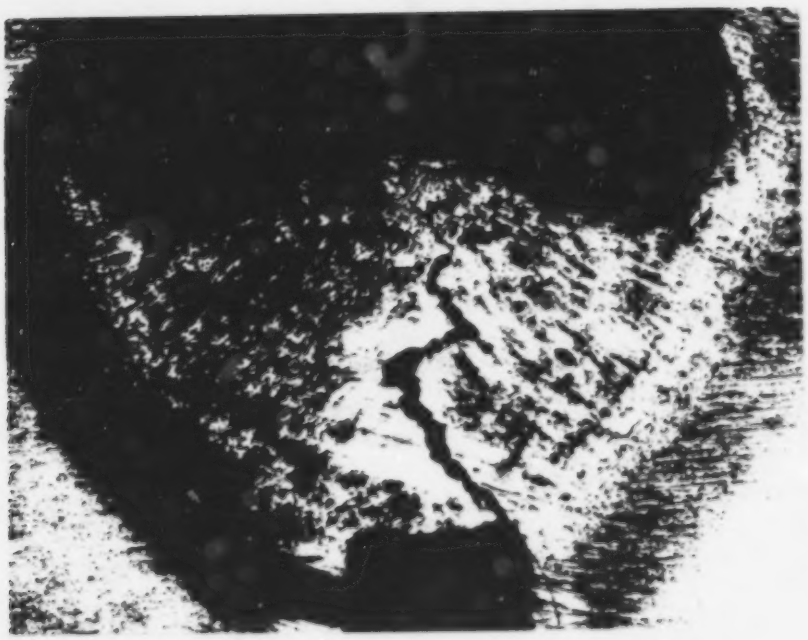

57B

Figure 14 (c): Cross-Section of cracked restraint test weld, steel 13D, room temperature

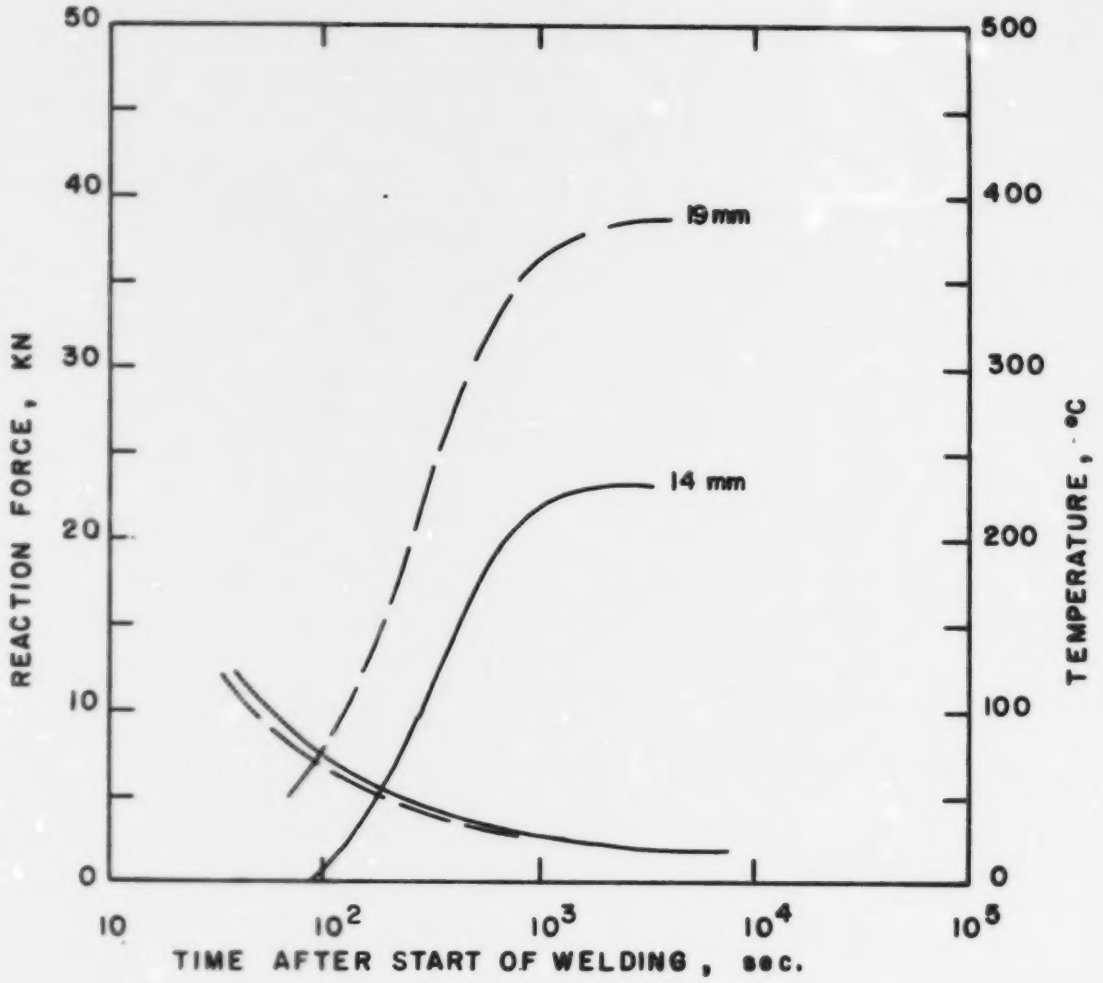

Figure 15 (a) - Relationship between reaction force and time after start of welding. welds made at room temperature, high restraint

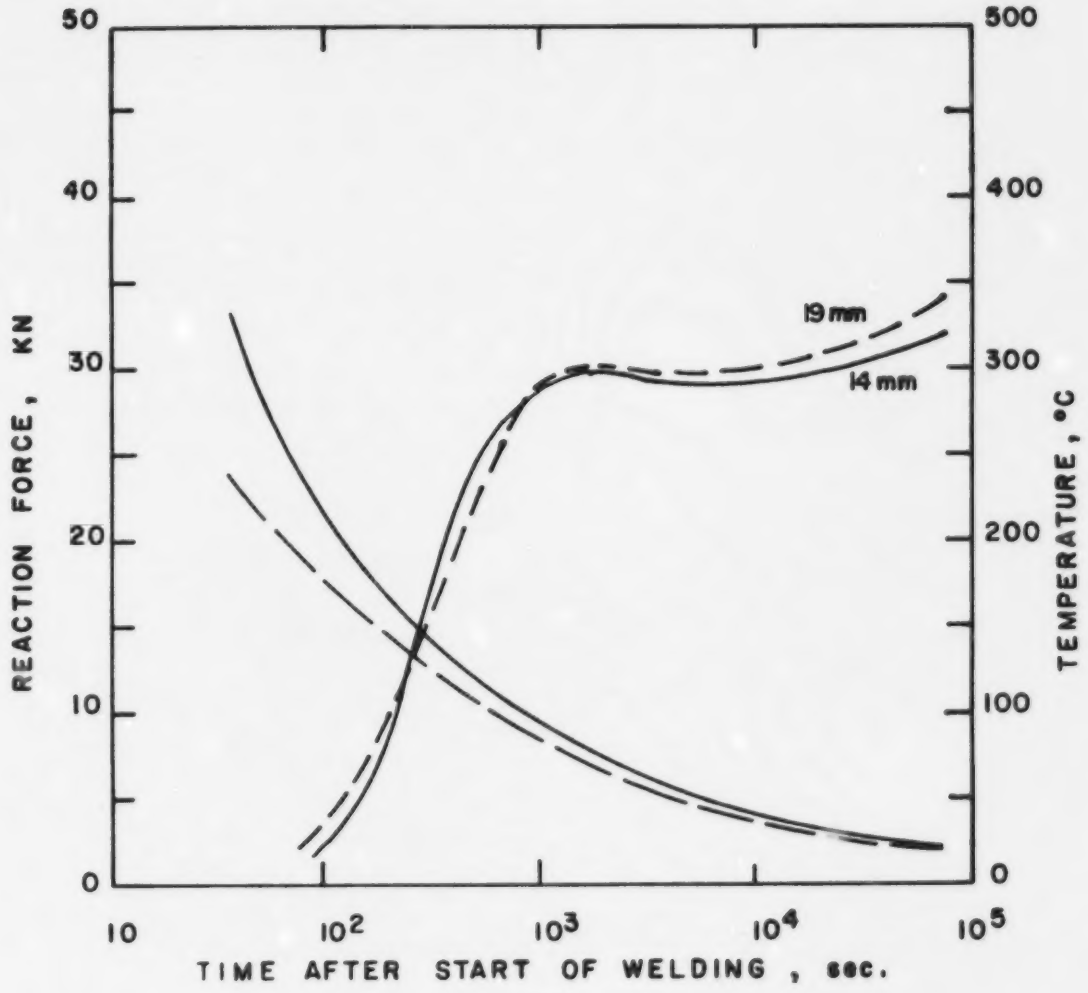

Figure 15 (b) - Relationship between reaction force and time after start of welding, preheat of 60°C above room temperature, high restraint

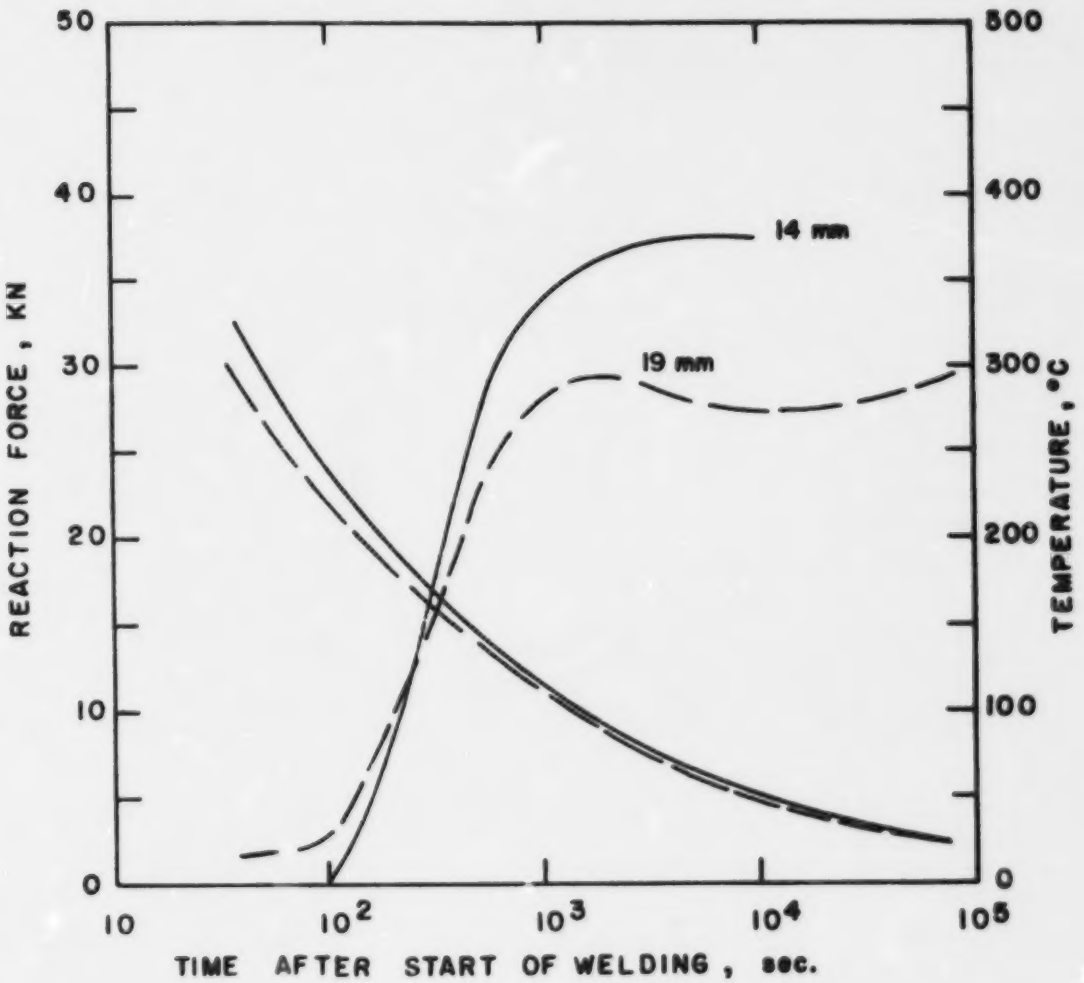

Figure 15 (c) - Relationship between reaction force and time after start of welding, preheat of 100°C above room temperature, high restraint.

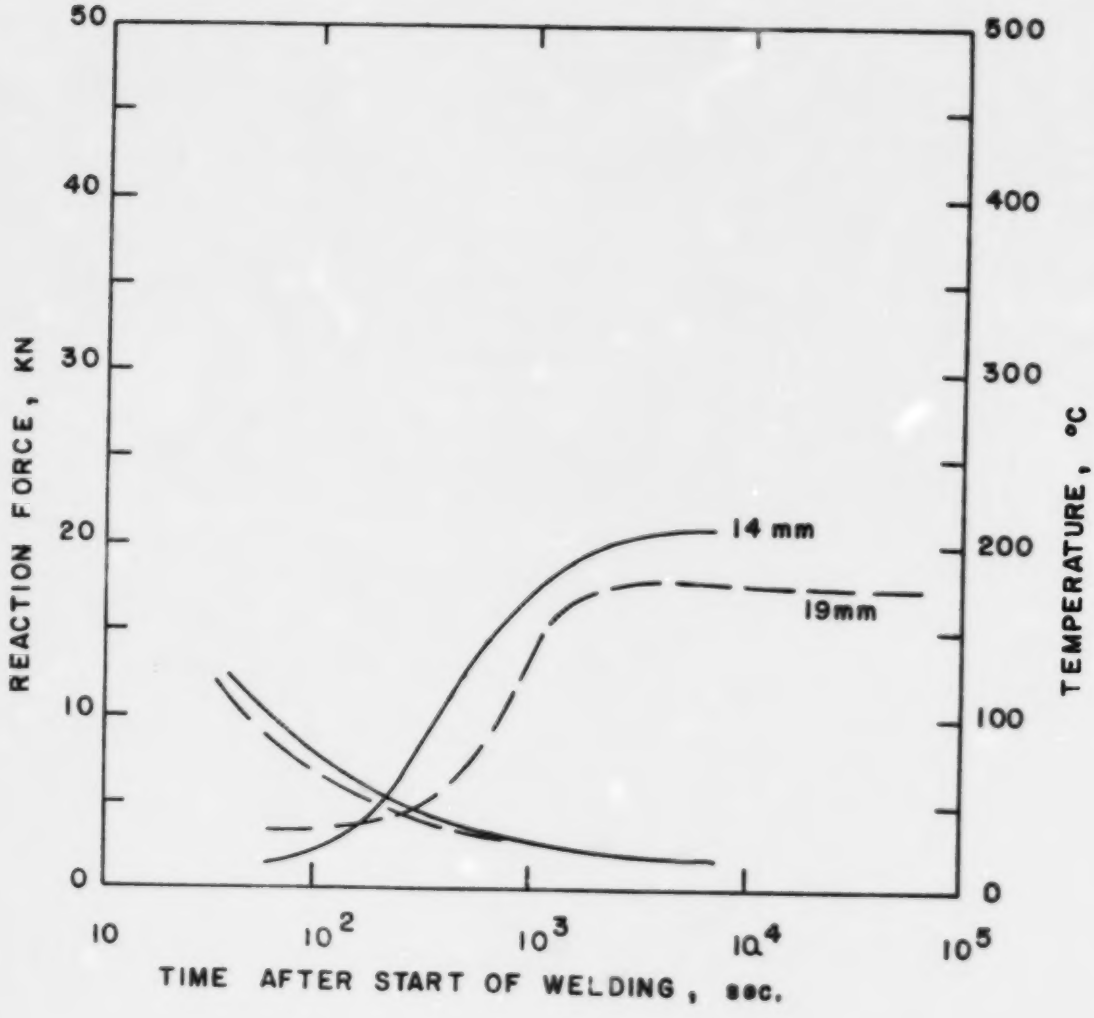

Figure 15 (d) - Relationship between reaction force and time after start of welding, welds made at room temperature, low restraint.

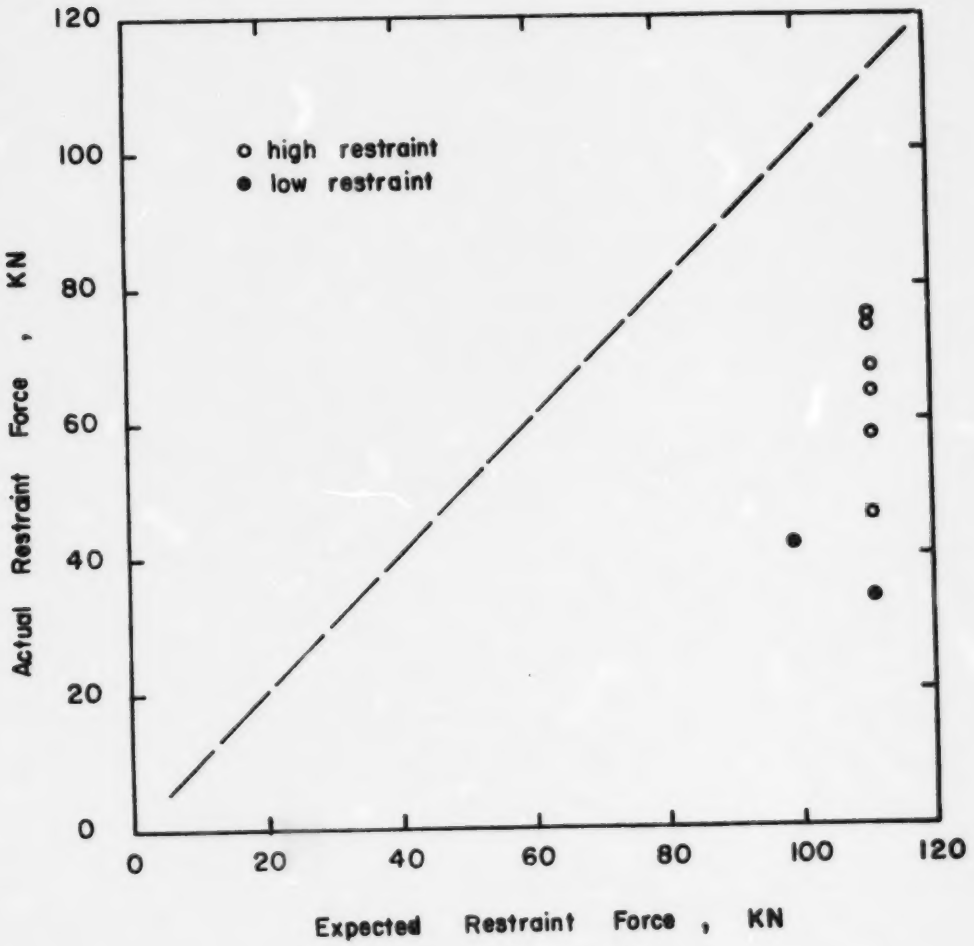

Figure 16: Comparison of Calculated and Measured reaction forces for instrumented restraint tests

APPENDIX A

MODIFIED IMPLANT CALIBRATION

APPENDIX A

MODIFIED IMPLANT CALIBRATION

The strain produced in the implant specimen as a function of torque was determined in a preliminary set of experiments, and is shown in Figure A1. The values shown represent different combinations of nuts and bearings. It can be seen that the range of strains for a given torque is within acceptable limits. This was accomplished by retapping all nuts and discarding those which were beyond ±10% of the average strain at 576 mm-kg torque.

The strain was also calibrated against uniaxial tension in a Hounsfield tensometer to provide a check as to whether the thrust bearing was effective to eliminate the torque. A load of 45.35 kg produced a strain of 73 με this result was linear up to a load of 453.5 kg. The strain gauges were mounted on a length whose cross-sectional area is 31.67 mm^2. For 453.5 kg load, the stress can be found to be:-

$$\sigma = \frac{F}{A} = \frac{453.5}{31.67} = 14.32 \ \frac{kg}{mm^2}$$

Assuming E = 21000 kg/mm^2, the stress can be calculated to be

$$\sigma = \varepsilon E = 730 \times 10^{-6} \times 21000 = 15.3 \ kg/mm^2$$

The difference is less than 7% between the calculated and measured value, which is within experimental variation.

The torque required to produce a strain 730 με is found from Figure A1 to be 626.7 mm-kg. Based on the nominal diameter of the implant specimen, a torque coefficient can be calculated:-

$$K = \frac{T}{Fd} = \frac{626.7}{453.5(6.35)} = 0.2176$$

This value depends on both geometry and the friction between threads (i.e., $K = 0.126 + 0.625\ \mu_c$ is the friction coefficient between threads): μ_c was found to be 0.15. Typical values range from 0.15 to 0.25. It is felt that μ_c is low enough to reduce variations between subsequent loadings and high enough to prevent the load from relaxing.

The actual tensile stress area for 1/4"-UNF 32 threads is 23.5 mm^2. This would increase the stress for the implant to:-

$$\sigma = \frac{F}{23.5}$$

but $$F = \frac{T}{Kd} = \frac{T}{0.2176(6.35)} = .724\ T, \text{ and}$$

σ = tensile stress, kg/mm^2

T = torque, mm-kg

Therefore the calibration of the implant specimens has shown that there is a unique relationship between stress and torque which is given above.

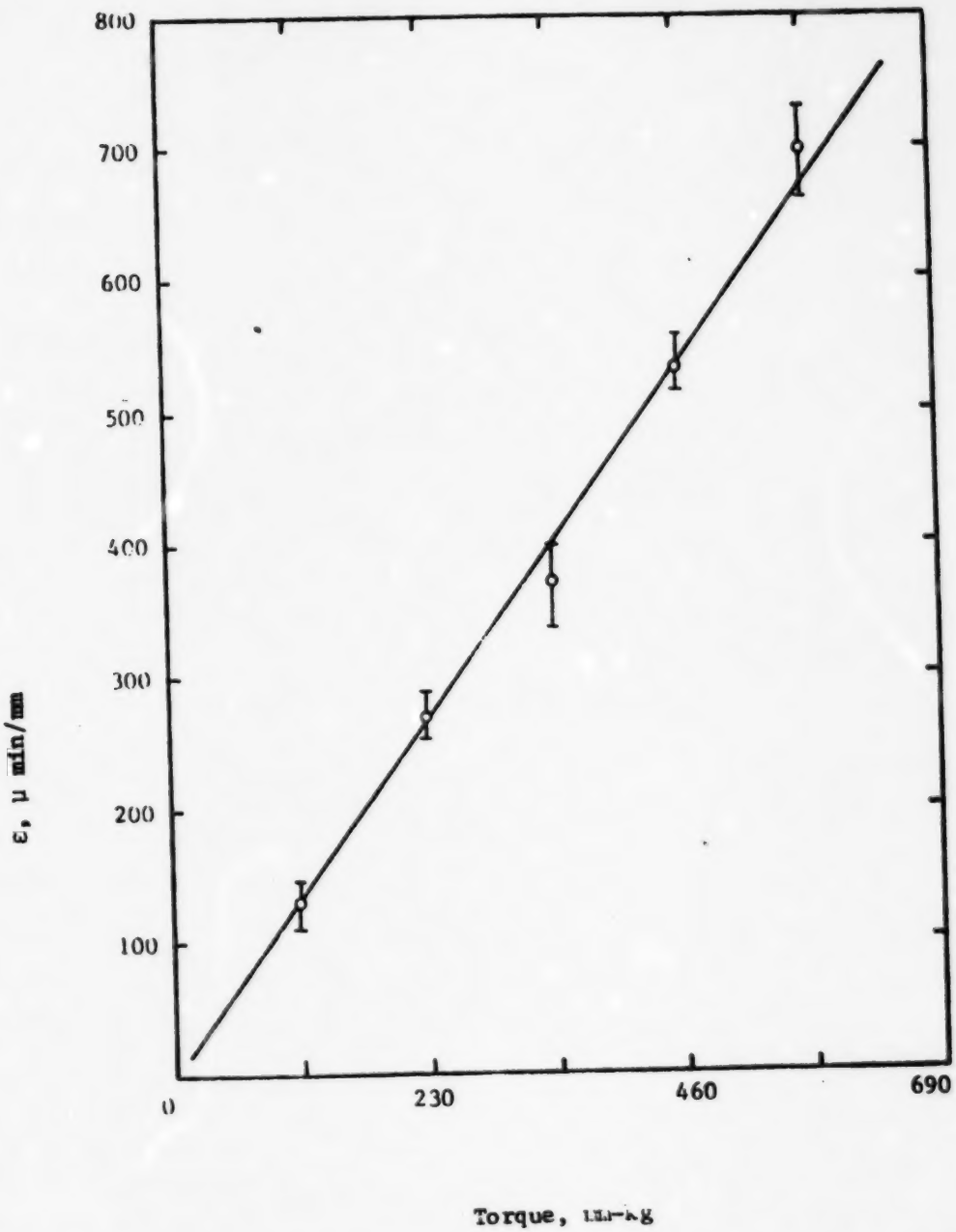

Figure A1 - Results of Strain vs. Torque Calibration of Strain Gauge Implant

A P P E N D I X B

G-BOP RESULTS

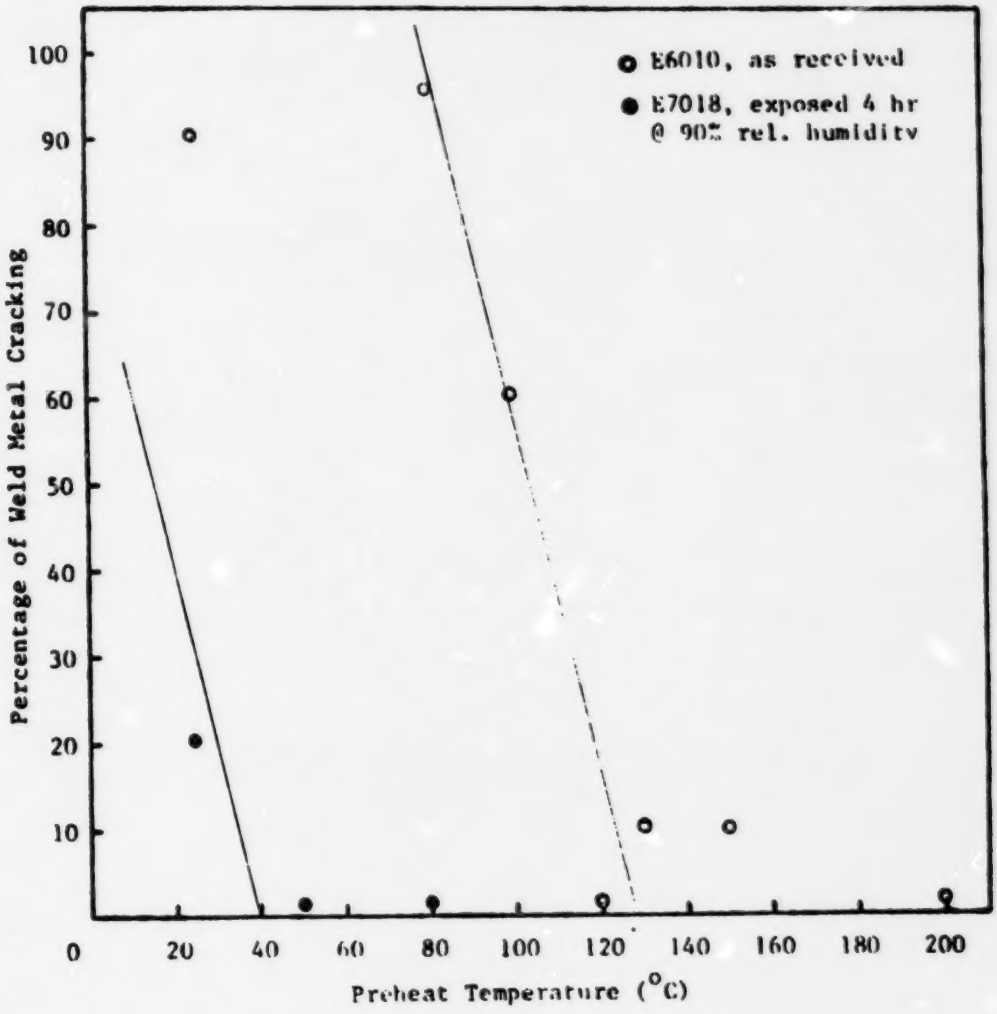

Figure B1: Weld Metal Cracking Percentage vs. preheat temperature for steel.131

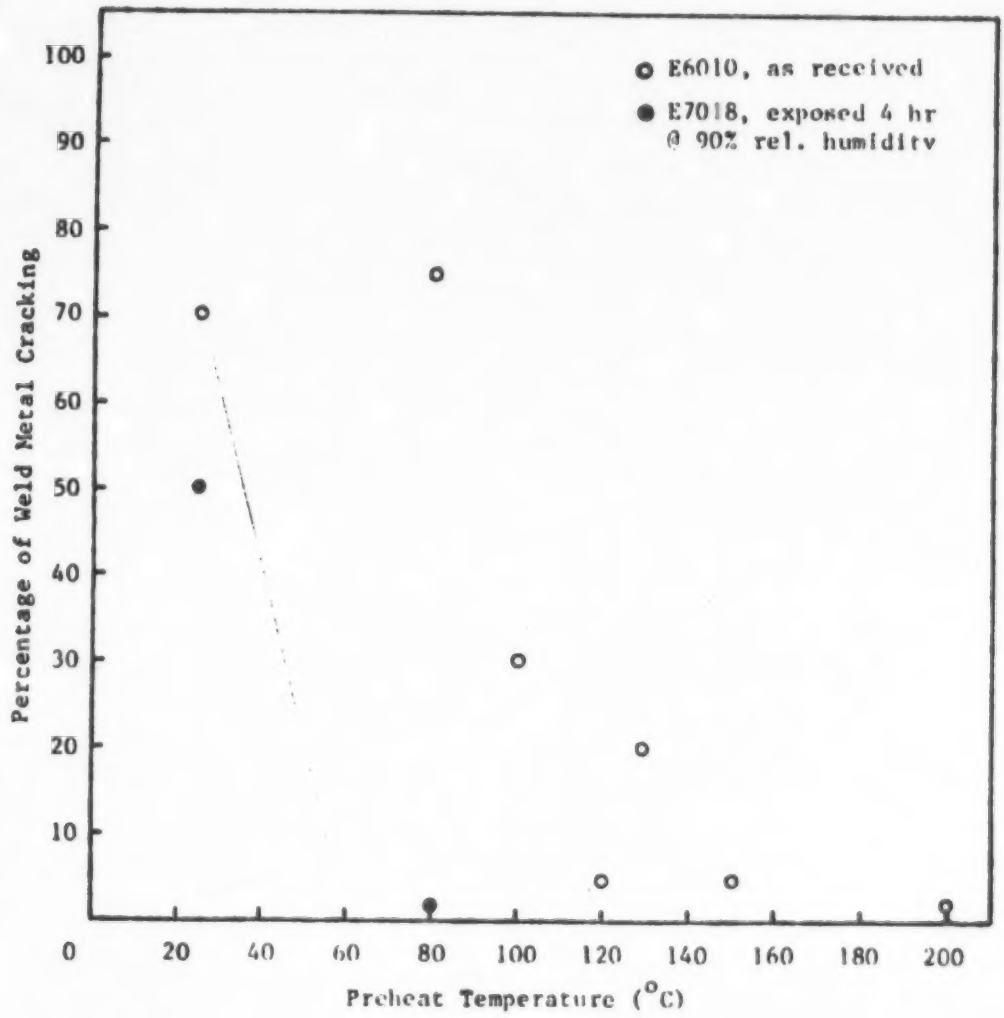

Figure B2: Weld Metal Cracking percentage vs. preheat temperature for steel 132

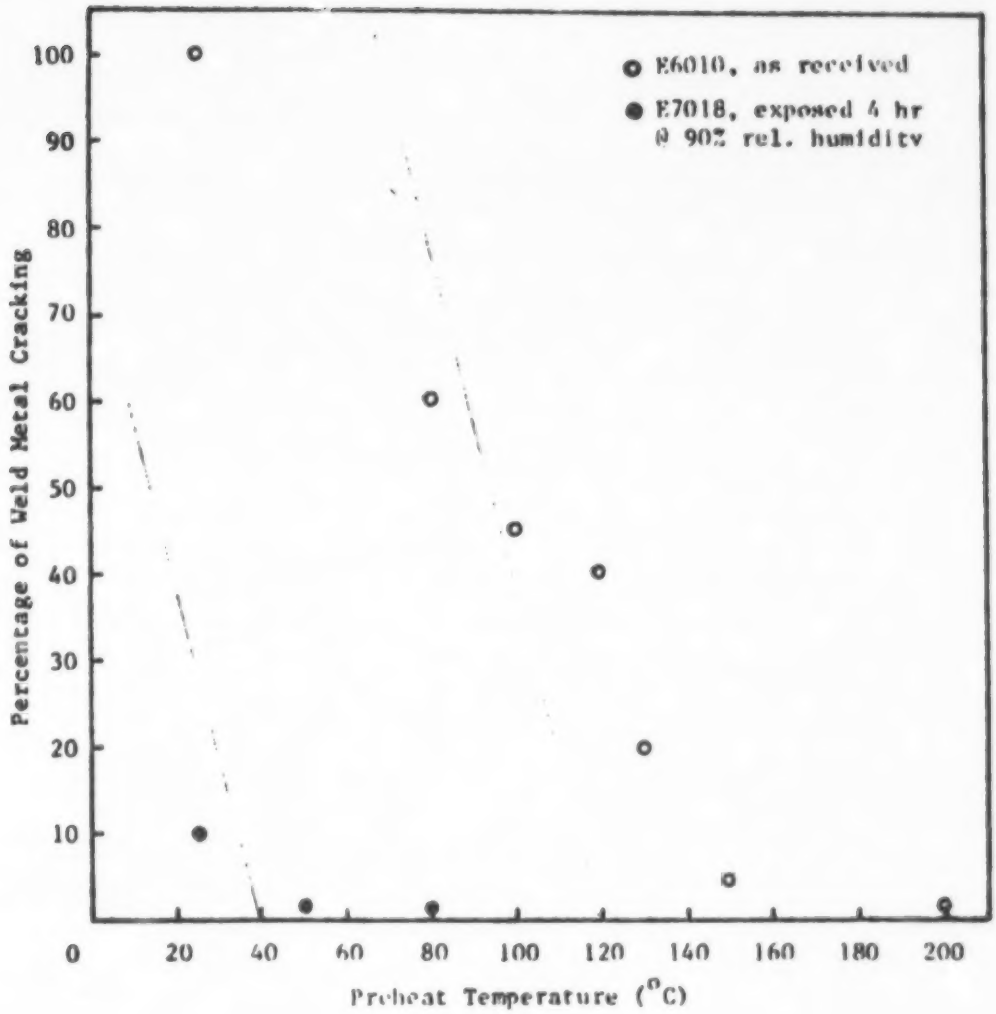

Figure B3: Weld metal cracking percentage vs. preheat temperature for steel 133

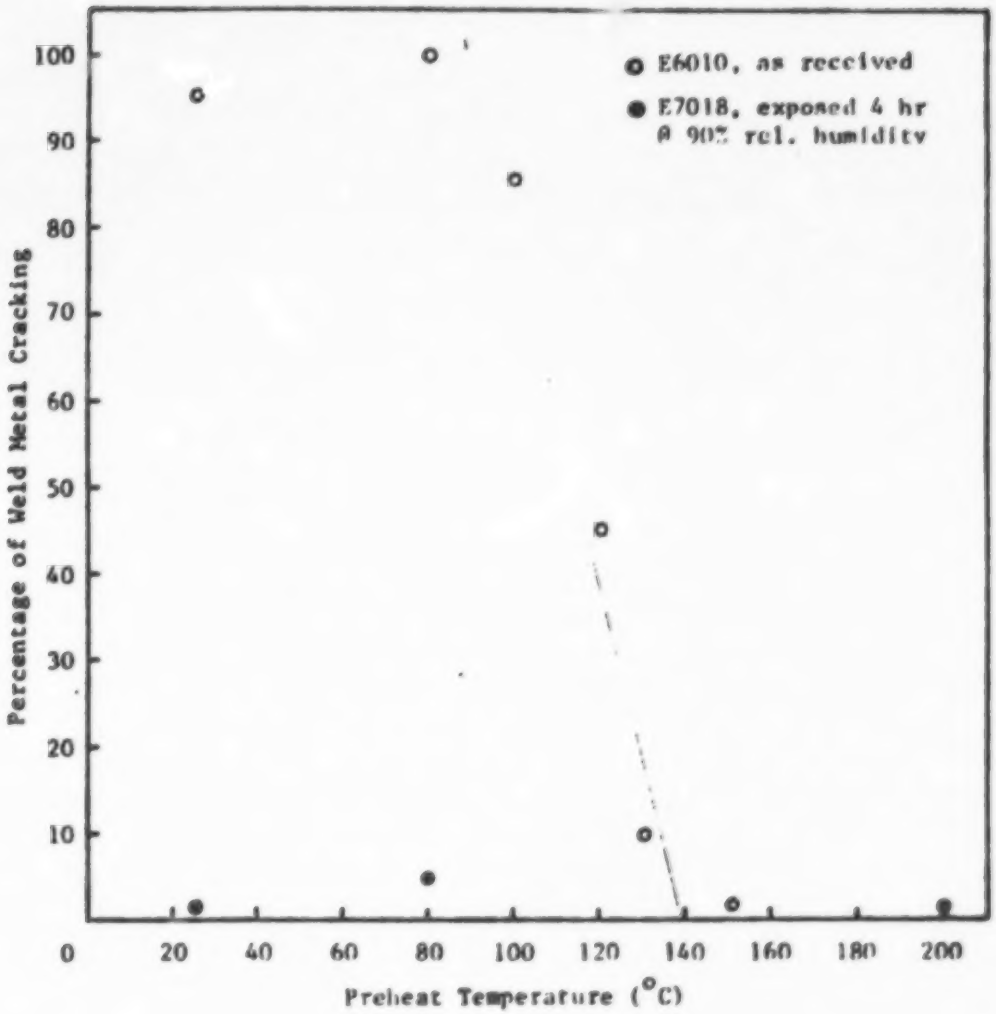

Figure B4: Weld metal cracking percentage vs. preheat temperature for steel 134

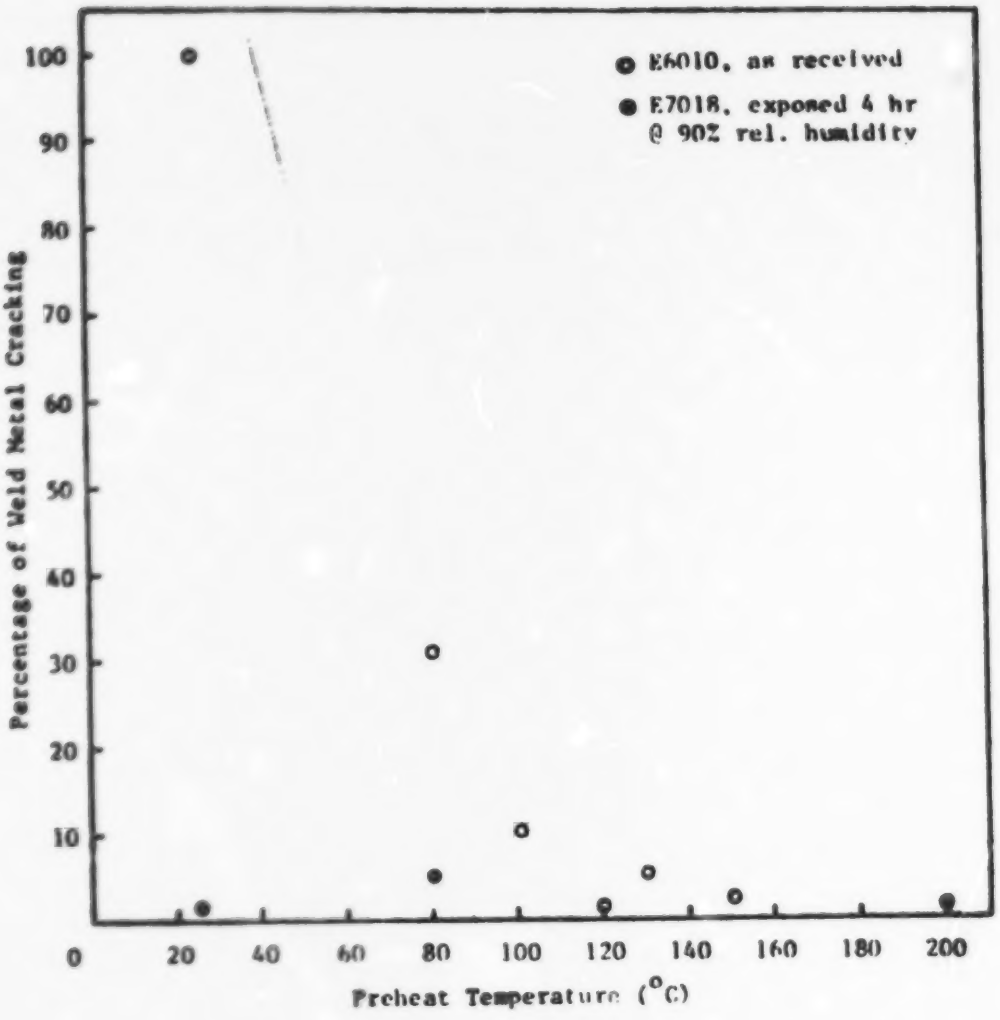

Figure B5: Weld metal cracking percentage vs. preheat temperature for steel 135

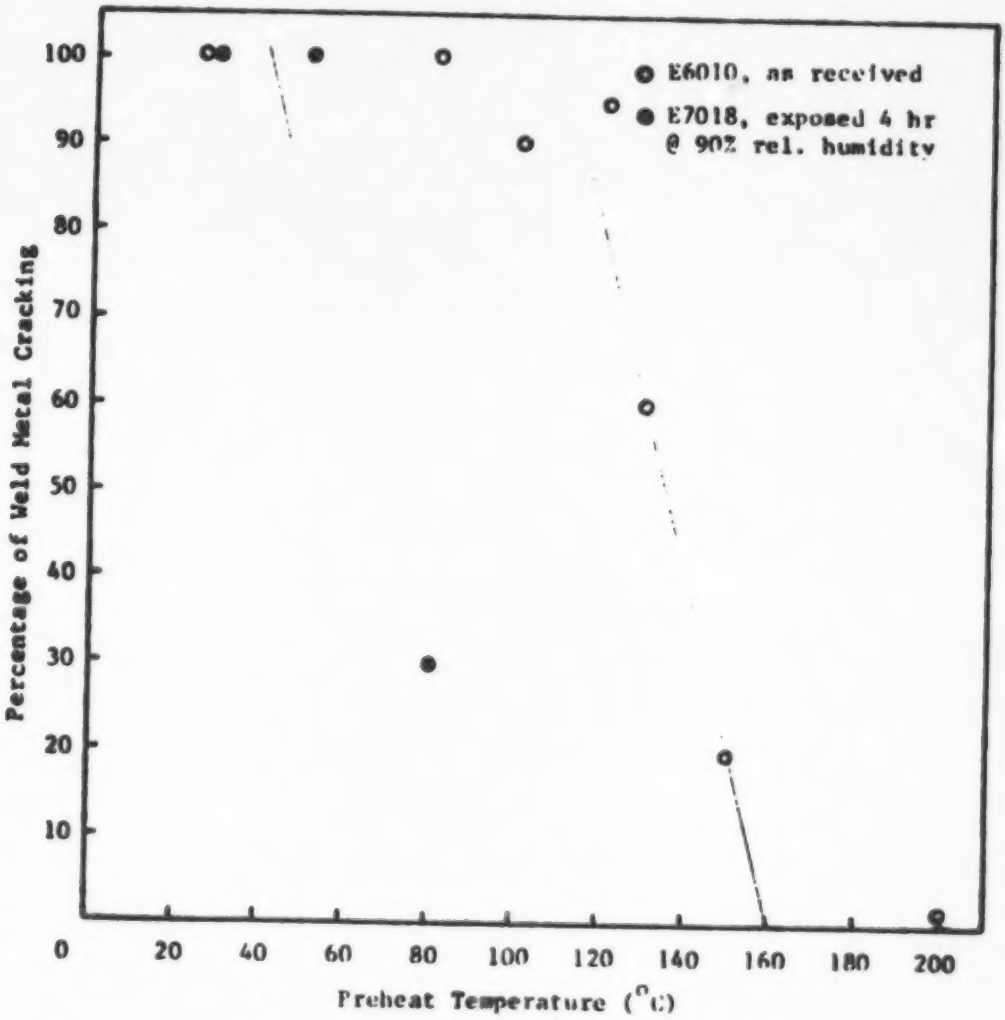

Figure B6: Weld metal cracking percentage vs preheat temperature for steel 136

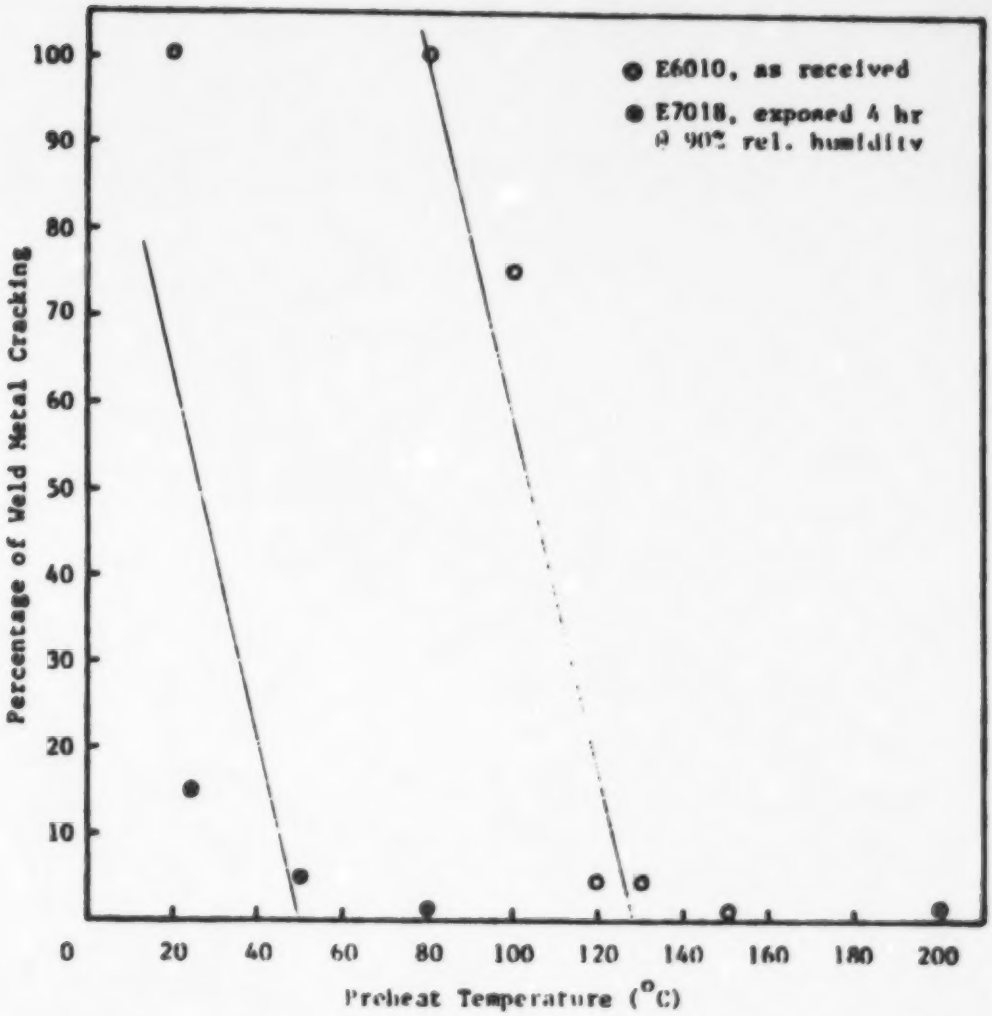

Figure B7: Weld metal cracking percentage vs. preheat temperature for steel 137

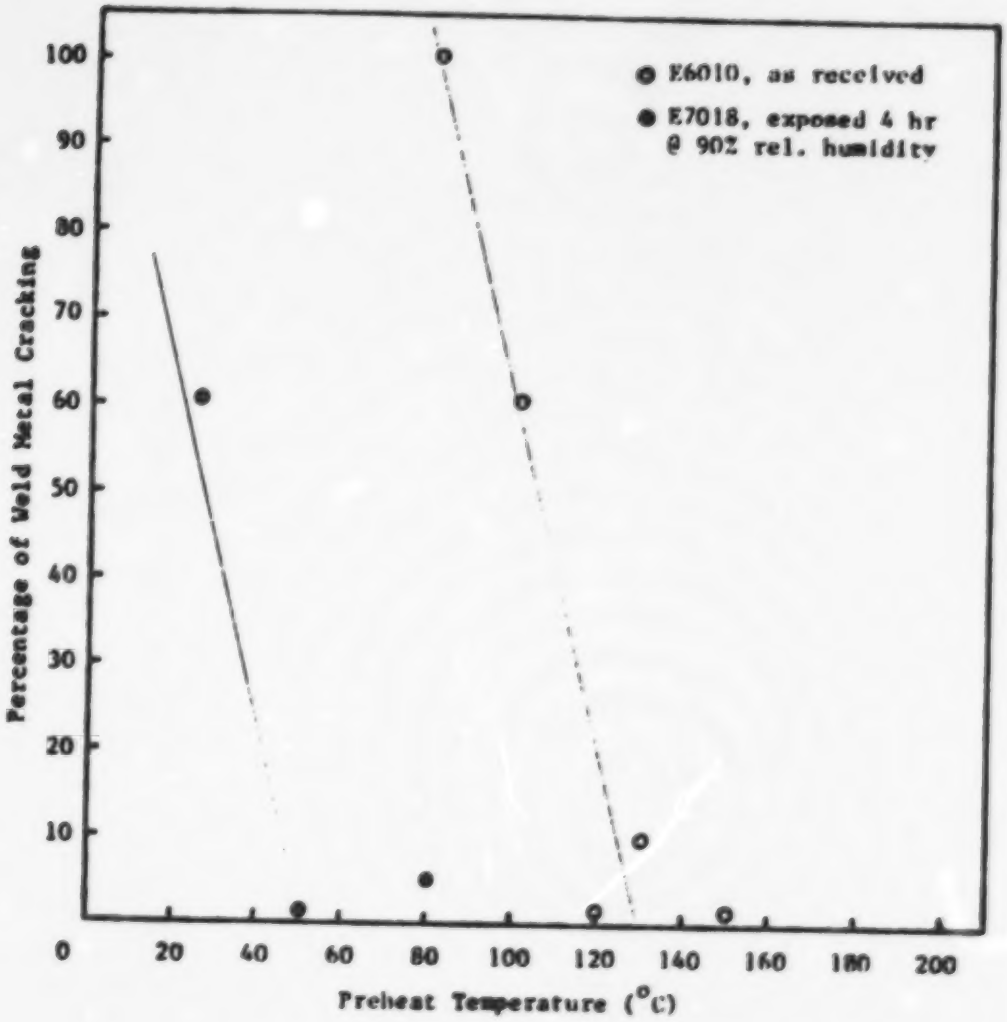

Figure B8: Weld metal cracking percentage vs. preheat temperature for steel 138

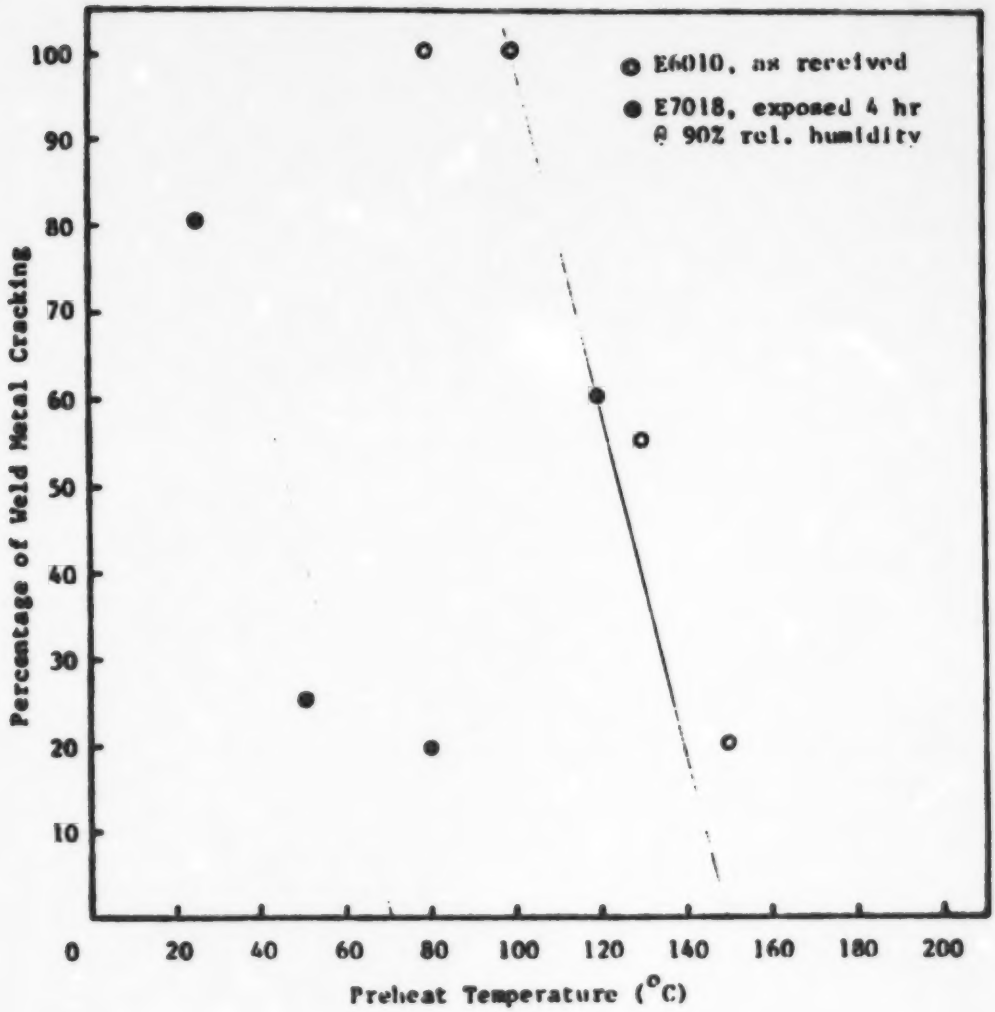

Figure B9: Weld metal cracking percentage vs. preheat temperature for steel 139

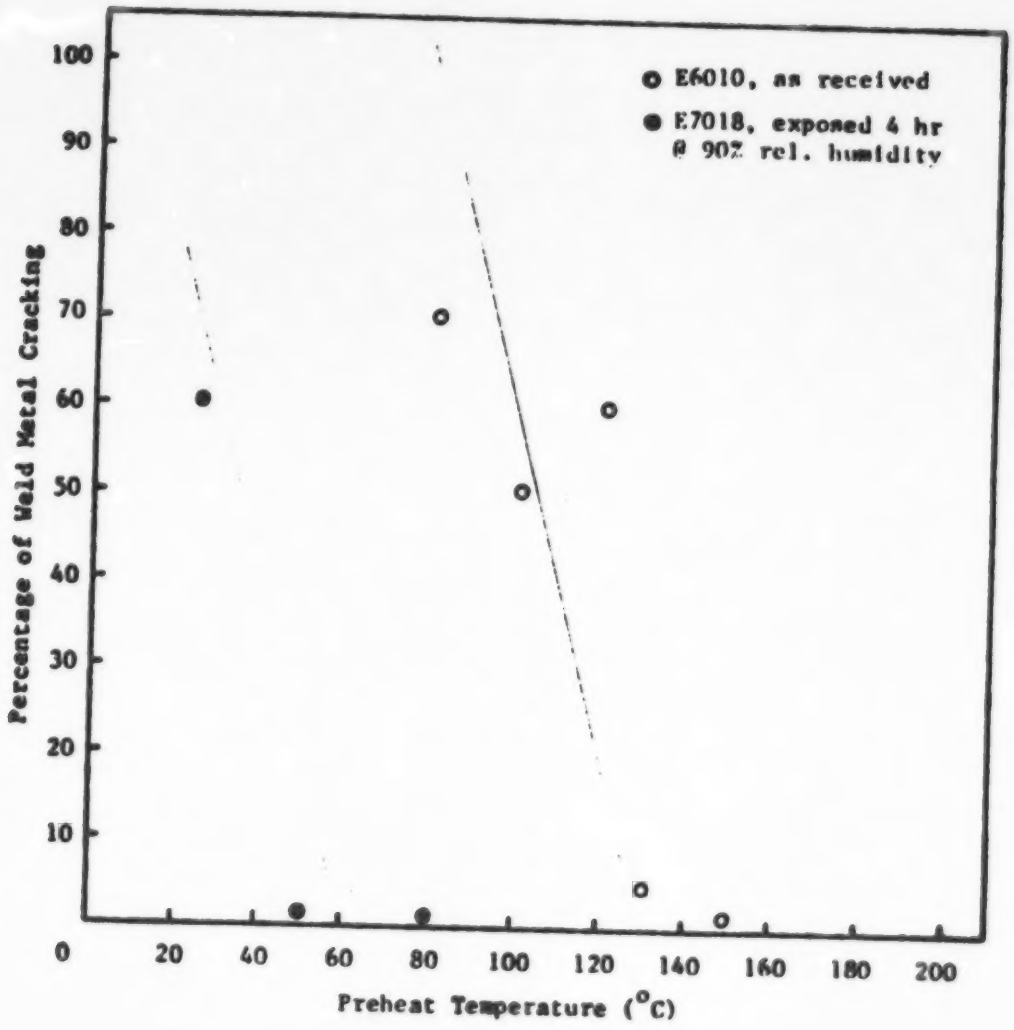

Figure B10: Weld metal cracking percentage vs. preheat temperature for steel 1310

APPENDIX C

STATISTICAL ANALYSIS OF WELD METAL CRACKING TESTS

Preheat °C	Alloy No. 131	132	133	134	135	136	137	138	139	1310	Total T_i	Mean $\bar{x}_i$	Variance s^2_i
20	90	70	100	95	95	100	100	100	100	100	950	95.0	88.9
80	95	75	60	100	30	100	100	100	100	70	830	83.0	573.0
100	60	30	45	85	10	90	75	60	100	50	605	60.5	786.0
120	0	5	40	45	0	95	5	0	60	60	310	31.0	1143.0
130	10	20	20	10	5	60	5	10	55	5	200	20.0	422.0
150	10	5	5	5	5	20	0	5	20	0	75	7.5	51.0
	265	205	270	340	145	465	285	275	435	285	2970		TOTAL, t_i
	44.2	34.2	45.0	56.7	24.2	77.5	47.5	45.8	72.5	47.5			Mean, $\bar{x}_i$
	1841	971	1100	1822	1312	1018	2428	2228	1098	1498			Variance, s^2_i

$$T = \sum_{i=1}^{c} T_i = 2970 \qquad \bar{x} = \frac{T}{cn} = \frac{2970}{60} = 49.5$$

$$\sum_{i,j} x^2_{i,j} = 237500$$

TWO-WAY ANOVA - Chemical Composition

$$\text{Correction factor} = \frac{T^2}{cr} = \frac{2970^2}{10(6)} = 147015$$

$$\text{Total corrected sume of squares} = 237500 \quad \sum_{i,j} x^2_{i,j}$$
$$-147015$$
$$90485$$

$$\text{Treatment sum of squares} = \frac{1}{6} \sum_{i=1}^{10} T^2_i - 147015 = 160883 - 147015$$
$$= 13868$$

$$\text{Block sum of squares} = \frac{1}{10} \sum_{i=1}^{6} T^2_i - 147015 - 209915 - 147015 = 62900$$

Source	Sum of Squares	df	Mean Square	F. ratio
Treatments	13868	9	1540.9	5.06
Blocks	62900	5	12580.0	41.27
Residual	13717	45	304.8	
Total	90485	59		

$F_{0.05,9,45} = 2.10$

$F_{0.05,5,45} = 2.43$

- both chemical composition and preheat are significant

The calculated F-ratio and value from tables for the F-distribution are given below to show the significance of relaxing certain alloys.

Alloy Removed	F-Ratio Calculated	Table	Significance of Composition
135	4.475	2.18	YES
136	3.88	2.18	YES
135, 136	3.22	2.29	YES
135, 136, 139	1.11	2.42	NONE
136, 139	2.06	2.29	NONE

APPENDIX D

HIGH RESTRAINT CRACKING RESULTS

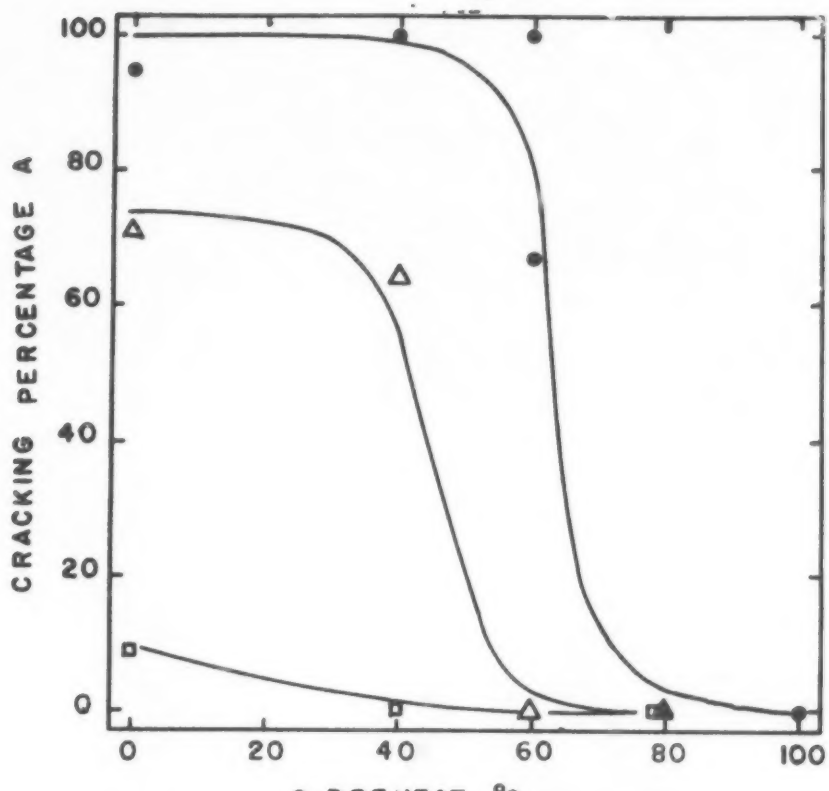

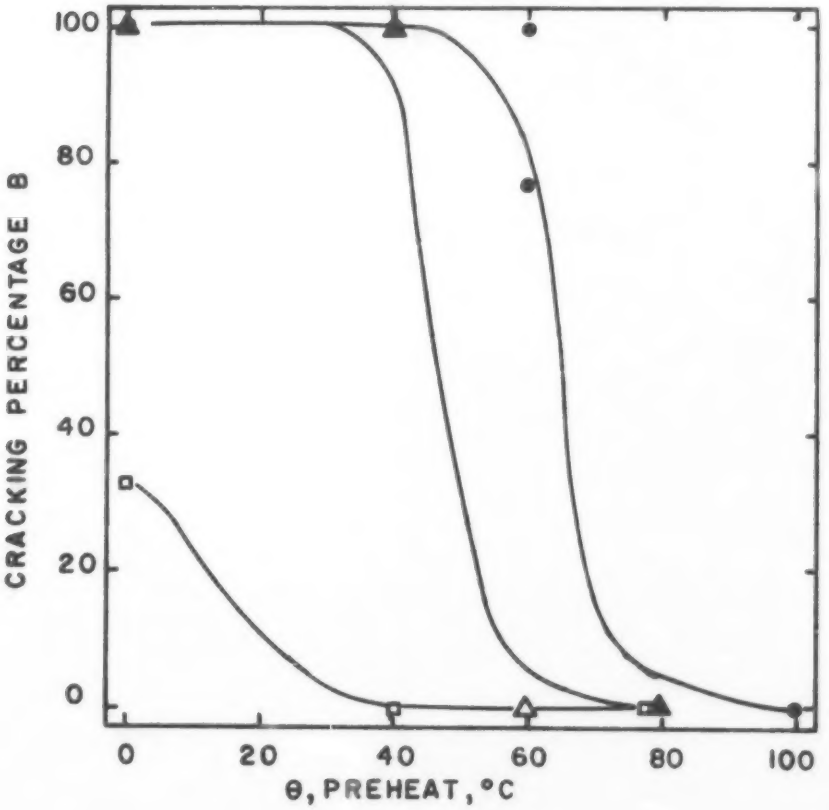

Figure D1 a) Cracking Percentage A vs. preheat for steel 13A
b) Cracking Percentage B vs. preheat for steel 13A

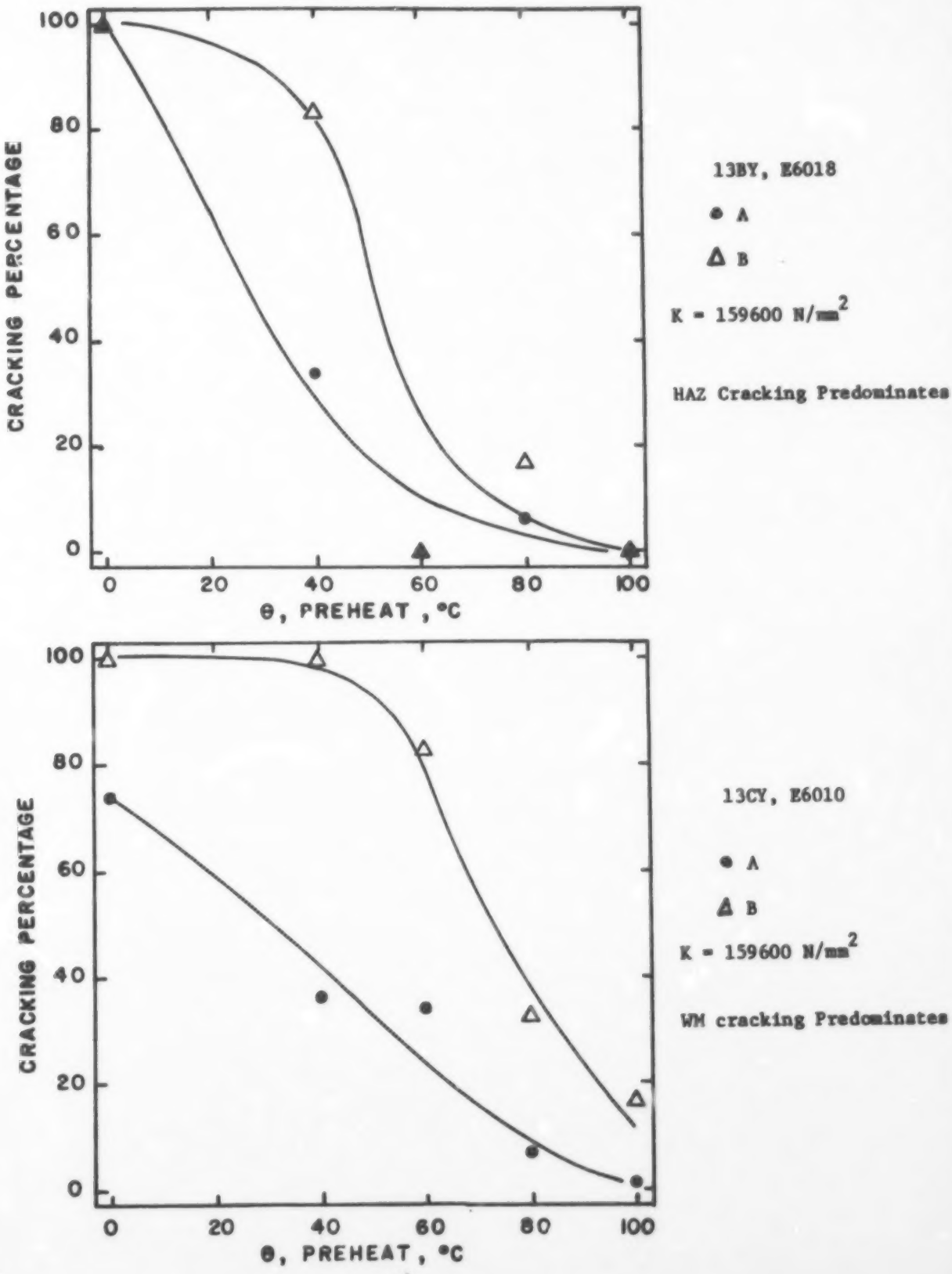

Figure D2 - (above) Cracking percentage vs preheat for steel 13B
D3 (below) Cracking percentage vs preheat for steel 13C

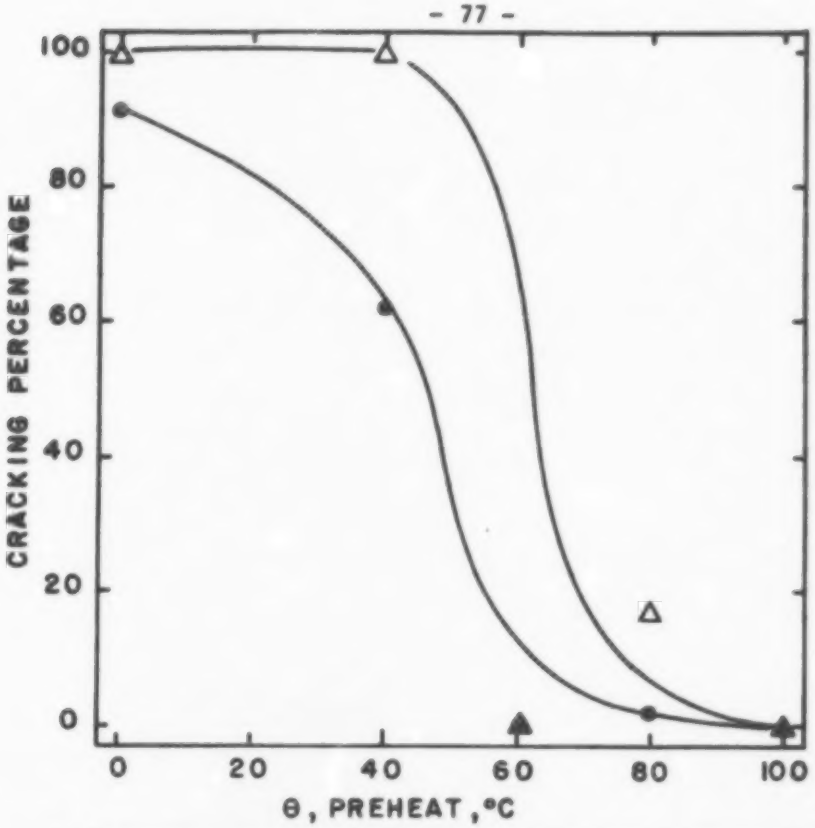

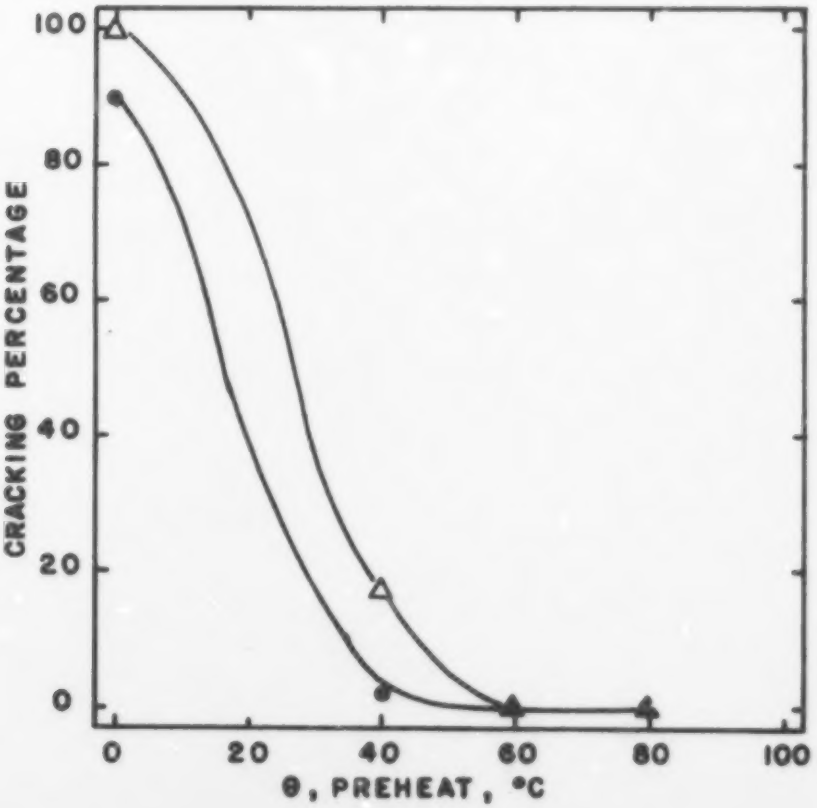

Figure D4 - (above) Cracking precentage vs preheat for steel 13D
FigureD5 (below) Cracking percentage vs preheat for steel 13E

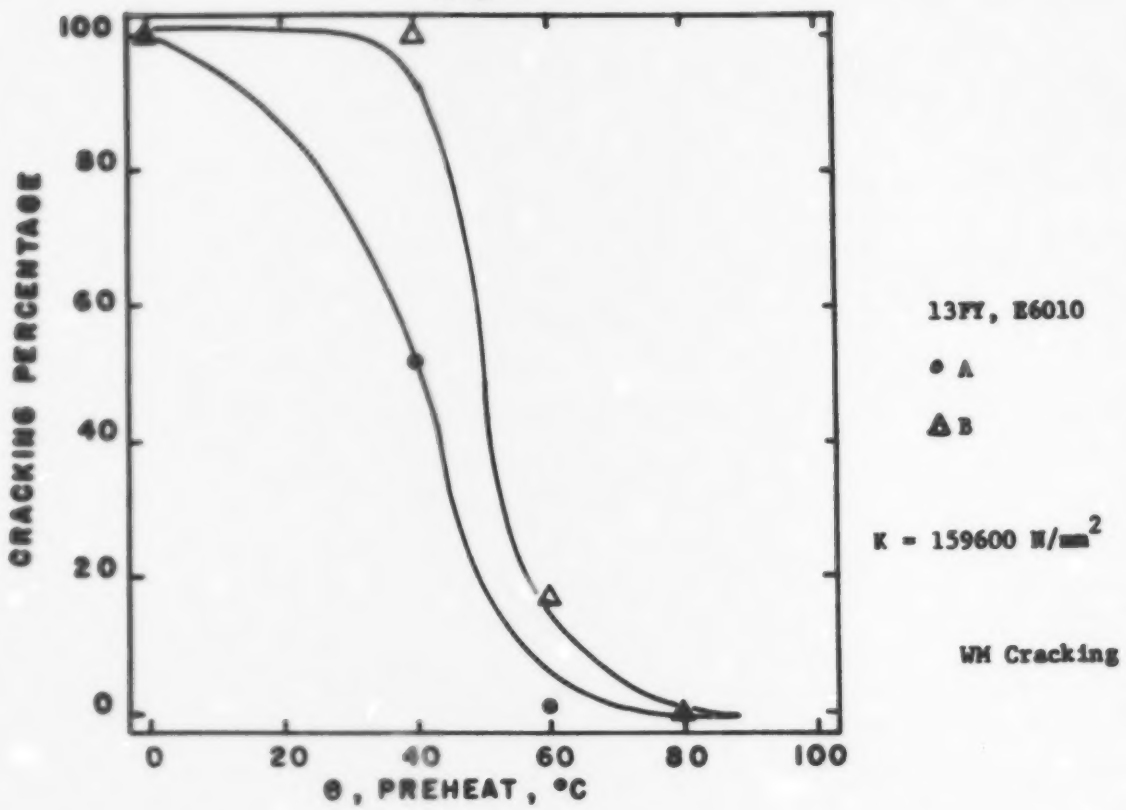

Figure B6 - Cracking percentage vs preheat for steel 13F